Asian Journal of Pharmaceutical Sciences 18 (2023) 100783

Available online at www.sciencedirect.com

ScienceDirect

journal homepage: www.elsevier.com/locate/AJPS

Original Research Paper

Selective ischemic-hemisphere targeting Ginkgolide B liposomes with improved solubility and therapeutic efficacy for cerebral ischemia-reperfusion injury

Yang Li[a,b], *Miaomiao Zhang*[a], *Shiyi Li*[a], *Longlong Zhang*[a], *Jisu Kim*[a], *Qiujun Qiu*[a], *Weigen Lu*[b,*], *Jianxin Wang*[a,*]

[a] *Department of Pharmaceutics, School of Pharmacy, Fudan University&Key Laboratory of Smart Drug Delivery, Ministry of Education, Shanghai, 201203, China*

[b] *National Pharmaceutical Engineering and Research Center, China State Institute of Pharmaceutical Industry, Shanghai 201203, China*

ARTICLE INFO

Article history:
Received 11 October 2022
Revised 23 December 2022
Accepted 24 January 2023
Available online 11 February 2023

Keywords:
Ginkgolide B
Cerebral ischemia reperfusion injury (CI/RI)
Docosahexaenoic acid
Liposomes
Brain targeting
Microglia

ABSTRACT

Cerebral ischemia-reperfusion injury (CI/RI) remains the main cause of disability and death in stroke patients due to lack of effective therapeutic strategies. One of the main issues related to CI/RI treatment is the presence of the blood-brain barrier (BBB), which affects the intracerebral delivery of drugs. Ginkgolide B (GB), a major bioactive component in commercially available products of *Ginkgo biloba*, has been shown significance in CI/RI treatment by regulating inflammatory pathways, oxidative damage, and metabolic disturbance, and seems to be a candidate for stroke recovery. However, limited by its poor hydrophilicity and lipophilicity, the development of GB preparations with good solubility, stability, and the ability to cross the BBB remains a challenge. Herein, we propose a combinatorial strategy by conjugating GB with highly lipophilic docosahexaenoic acid (DHA) to obtain a covalent complex GB-DHA, which can not only enhance the pharmacological effect of GB, but can also be encapsulated in liposomes stably. The amount of finally constructed Lipo@GB-DHA targeting to ischemic hemisphere was validated 2.2 times that of free solution in middle cerebral artery occlusion (MCAO) rats. Compared to the marketed ginkgolide injection, Lipo@GB-DHA significantly reduced infarct volume with better neurobehavioral recovery in MCAO rats after being intravenously administered both at 2 h and 6 h post-reperfusion. Low levels of reactive oxygen species (ROS) and high neuron survival *in vitro* was maintained via Lipo@GB-DHA treatment, while microglia in the ischemic brain were polarized from the pro-inflammatory M1 phenotype to the tissue-repairing M2 phenotype, which modulate neuroinflammatory and angiogenesis. In

* Corresponding authors.
E-mail addresses: luweigen@sinopharm.com (W. Lu), jxwang@fudan.edu.cn (J. Wang).
Peer review under responsibility of Shenyang Pharmaceutical University.

https://doi.org/10.1016/j.ajps.2023.100783

addition, Lipo@GB-DHA inhibited neuronal apoptosis via regulating the apoptotic pathway and maintained homeostasis by activating the autophagy pathway. Thus, transforming GB into a lipophilic complex and loading it into liposomes provides a promising nanomedicine strategy with excellent CI/RI therapeutic efficacy and industrialization prospects.

1. Introduction

According to the World Health Organization (WHO), in 2019 stroke was responsible for approximately 11% of total deaths and ranked among the top 10 leading causes of death [1]. Acute ischemic stroke (AIS), caused by sudden thrombus blockage in blood vessels, is the most common subtype of stroke [2]. The restoration of the blood supply, referred to as "reperfusion," is a vital method for AIS treatment. However, reperfusion intervention commonly leads to the occurrence of cerebral ischemia-reperfusion injury (CI/RI) and survivors still face complications that may develop into disabilities, mainly caused by secondary reperfusion followed by ischemia due to the production of oxidative stress and excess inflammatory cytokines [3].

To alleviate post-ischemia reperfusion injury, a variety of drugs, including gamma-aminobutyric acid (GABA) receptor agonists, NO-related interventions, nonsteroidal anti-inflammatory drugs (NSAIDs), and neuroprotective agents, have been used in clinical and preclinical research [4–6]. However, none of these strategies can completely prevent ongoing neuroinflammation because of the complexity of CI/RI. Inflammatory responses after stroke occur and persist throughout the brain due to excessive oxygen free radicals and the infiltration of peripheral immune cells after reperfusion. These can also aggravate secondary brain injury by exacerbating blood-brain barrier (BBB) damage and microvascular dysfunction, inducing neuronal cell death [7] and causing irreversible damage. Now, studies on cerebral ischemia injury treatment have mainly been limited to the recovery of neuron themselves, or different separated cell populations and structures in the brain, ignoring the root cause of ROS and integrity of brain function. Therefore, the overall remodeling of the neurovascular unit (including neuron, glia, and blood vessels) and the comprehensive regulation of the inflammatory microenvironment are believed to be more effective, and are urgently needed.

Ginkgo biloba (*G. biloba*) extract products have been widely used to prevent and treat stroke for many years due to their potential to decoy neuronal apoptosis and regulate neuroinflammation [8]. For example, oral pretreatment with *G. biloba* extracts has been shown to significantly decrease the level of malondialdehyde (MDA) and brain edema in a dose-dependent manner after cerebral ischemia [9]. It has also been proved to be beneficial to cognitive recovery, which is of great significance for high incidence of cognitive disorders after stroke [10]. Here, the main active ingredients of *G. biloba* leaf extract are diterpene lactones, including ginkgolides A, B, C and K. Among them, ginkgolide B (GB) has the strongest activity in treating cerebrovascular diseases, which can block inflammatory responses by participating in platelet-activating factor (PAF)-mediated signal transduction and attenuate neuronal damage induced by regulating the miR-206/BDNF signaling pathway [11,12]. Moreover, GB seems to play a positive role in the differentiation of neural stem cells after stroke by upregulation of SOCS2 to furtherly activate EGF receptor [13]. So, GB was selected as a candidate drug in this paper. Besides, *G. biloba* diterpene lactone meglumine injection (referred to GB injection in this study), extracted from *G. biloba* containing over 50% GB and other diterpene lactones, was chosen as a positive control. The therapeutic effect of this injection plus aspirin has also been clinically validated for vascular recanalization and neuron recovery after stroke [14].

Previous reports have demonstrated that GB can inhibit persistent inflammatory response and stimulate neuron regeneration after stoke, which are the core events of CI/RI. However, due to the existence of the blood-brain barrier (BBB), the insufficient targeted accumulation of GB in the damaged hemisphere via noninvasive administration restricts treatment outcomes. For example, after 4 h of reperfusion, the intravenous injection of GB could only downregulate the neurobehavioral score, and did little to mitigate neuroinflammation or reduce the cerebral infarction volume, indicating that the outcomes of this treatment are compromised with the therapeutic time window [15]. Several more deficiencies exist for GB injection in terms of the delivery of GB actively into the brain, including the accurate targeting of specific tissues or cells, deep penetration, and avoiding immune detection. Therefore, there is a need to overcome these shortcomings by developing a novel GB delivery system with improved therapeutic efficacy.

Multiple approaches have been reported to improve the efficiency of nanomedicine delivery to the damaged brain. Among various drug delivery systems, liposomes have shown great benefits for clinical translation because of their high biocompatibility, low toxicity, and high capacity for encapsulation in various cargos [16]. In addition, liposomes have advantages in post-stroke drug delivery because they can selectively aggregate in the ischemic hemisphere so as to a higher therapeutic agent accumulation [17]. Besides, a biphasic barrier enhancement and tight junction (TJ) abnormalities can be observed 48 h after stroke, which increases the paracellular permeability of molecules and liposomes. In addition, caveolin-mediated endocytosis and higher transcytosis rate greatly increases the transcellular transport of liposomes as early as 6 h of reperfusion and persists at least for 24 h [18,19]. Therefore, liposome may address the concerns of conventional GB injection, provide

enhanced brain-targeting ability, and be an ideal nanocarrier for GB delivery into the brain.

However, the LogP of GB is only 0.146, with a low hydrophilicity and lipophilicity [20], making it difficult to formulate GB in liposomes owing to poor encapsulation efficiency and stability. To solve the problem of the low lipophilicity of GB, we proposed strategies for forming covalent complexes with polyunsaturated fatty acids (PUFA) and subsequent liposomal encapsulation. In this study, docosahexaenoic acid (DHA) was chosen as it can be integrated into the lipid bilayer [21], thereby increasing the stability of the complex. For example, DHA has been already proposed to reconstruct cabazitaxel-DHA with the ability to be readily integrated into the lipid bilayer of liposomes for systemic administration [22]. And as reported, neuroprotection against cerebral ischemic stroke mediated by DHA includes improving neuronal defense capacity and inhibiting cellular inflammatory mechanisms by increasing the expression of nuclear factor erythroid 2-related factor 2 (Nrf2) and heme oxygenase 1 (HO-1), showing protective effects against oxidative stress-induced damage [23,24]. Besides, DHA can protect against post-stroke injury by regulating macrophage polarization [25–27], which suggests the possibility of a synergistic effect of GB and DHA. So, in this paper, DHA was finally chosen.

Here, we first synthesized GB-DHA to up-regulate the lipophilicity of GB and then loaded it into liposomes to increase its brain-targeting capability. The liposomes can further target the ischemic hemisphere of the brain to synergistically protect against neuron apoptosis via eliminating ROS, remodeling neurovascular unit via regulating the polarization of the pro-inflammatory and anti-inflammatory phenotype of microglia, and facilitating anti-inflammatory activity by reducing the infiltration of peripheral immune cells (Scheme 1). Our results validate this design rationale as a simple yet smart strategy for the development of GB as an effective medicine.

2. Materials and methods

2.1. Materials

Ginkgolide B (GB) was purchased from Dashbio, Inc. (Nanjing, China). Docosahexaenoic acid (DHA) was purchased from Macklin. Egg phosphatidylcholine (Egg PC, PL-100M) and 1,2-distearoyl-sn-glycero-3-phosphoethanolamine-N- [methoxy (polyethylene glycol) 2000] (DSPE-PEG_20) were purchased from AVT Pharmaceutical Co. Ltd. (Shanghai, China). The fluorescence dyes 1,1'-dioctadecyl-3,3,3′,3′-tetramethylindocarbocyanine perchlorate (Dil), 4-chlorobenzenesulfonate salt (DID), 1,1-dioctadecyl-3,3,3,3-tetramethylindotricarbocyanine (DiR), 4′,6-diamidino-2-phenylindole (DAPI), and the TUNEL apoptosis detection kit were purchased from Meilunbio (Dalian, China). Cholesterol, chloroform, methanol and Tween 80 were purchased from Sinopharm (Beijing, China). The ROS detection cell-based assay kit was purchased from Beyotime (Dalian, China). FITC anti-rat CD11b antibody, Alexa Fluor® 700 anti-rat CD45 antibody, and APC anti-rat CD3 were purchased from BioLegend (USA). PE anti-rat CD86 antibody was purchased from BD Biosciences. Rabbit anti-BDNF, rabbit anti-Bcl-2, and rabbit anti-Bax monoclonal antibodies were purchased from Abcam (Cambridge, UK). Rabbit anti-LC3B monoclonal antibody, rabbit anti-AMPKα1/α2 monoclonal antibody, and rabbit anti-ATG5 monoclonal antibody were purchased from Abclonal (Wuhan, China). Hieff® qPCR SYBR Green Master Mix (Low Rox Plus), and Hifair® II 1st Strand cDNA Synthesis Kit were purchased from Yeasen Biotechnology Co., Ltd. (Shanghai, China). The primers used for Q-PCR studies were synthesized by Sangon Biotech Co., Ltd. (Shanghai, China).

2.2. Cell lines and animals

PC12 neuron cells, and mouse microglia (BV2) were purchased from American Type Culture Collection (ATCC, USA) and cultured in DMEM medium supplemented with 10% fetal bovine serum (FBS), streptomycin (100 U/ml), and penicillin (100 U/ml) at 37°C in 95% air/5% CO2.

Male SD rats (180-250 g) were purchased from Shanghai JSS Laboratory Animal Co., Ltd. (Shanghai, China) and maintained under SPF conditions. All animal experiments were conducted in accordance with the guidelines evaluated and approved by the ethics committee of Fudan University.

2.3. Synthesis and characterization of GB-DHA

To improve the lipophilicity of GB, GB-DHA was synthesized according to a previously reported esterification method with modifications [28,29]. Briefly, GB (305 mg, 0.72 mmol) and DHA (196.8 mg, 0.6 mmol) were dissolved in acetonitrile (12 ml). Then, 1-(3-dimethylaminopropyl)-3-ethylcarbondiimine hydrochloride (EDC-HCl, 0.84 mmol) and 4-dimethylaminopyridine (DMAP, 0.12 mmol) was slowly added and the mixture was stirred for 1 h on ice. After stirring for 24 h under nitrogen gas condition, 30 ml ethylacetate replaced the organic solvents and then washed with 5% $NaHCO_3$ solution and saturated NaCl twice, respectively. Finally, the crude products were purified using column chromatography and washed with petroleum ether and ethyl acetate (7:3). The final structure was confirmed by ^{1}H-NMR spectroscopy using a 400 MHz system (400 MHz, Varian) and ESI-MS (QTRAP 6500+, SCIEX).

The log P of GB-DHA was tested by calculating the solubility in water and octanol (4:1). Briefly, water was saturated with n-octanol for 24 h, then 100 μg/ml GB-DHA was added to the mixed solution for 24 h continuously shaking at 25 °C. After holding for 12 h, the concentration of GB-DHA in water and n-octanol was tested by HPLC (Agilent 1200) respectively.

2.4. Preparation of Lipo@GB-DHA

GB-DHA-loaded liposomes (Lipo@GB-DHA) were prepared using the film dispersion method, as previously described [30,31]. Briefly, 15 mg EPC, 3 mg cholesterol, 1.5 mg DSPE-PEG_{2000}, and 1.73 mg GB-DHA (containing 1 mg GB) were dissolved in 2 ml chloroform. After removing organic solvent by rotary evaporation at 45 °C for 15 min, a thin film was formed and hydrated with 1 ml PBS at 45 °C for 60 min. Then, the suspensions were extruded through 400 nm and 200 nm

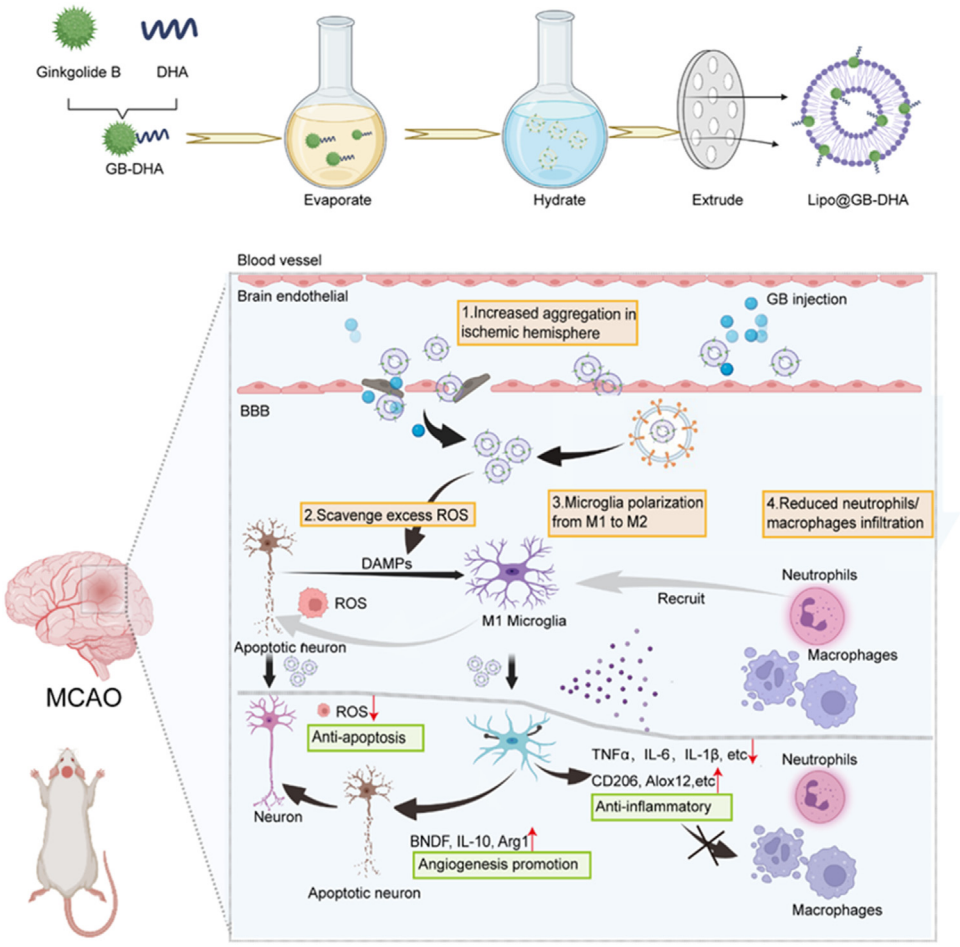

Scheme 1 – Schematic illustration of Lipo@GB-DHA therapy for cerebral ischemia. (1) Lipo@GB-DHA aggregated more in ischemic hemisphere, uptaken by caveolin over-expressed at ischemic hemisphere and carried by macrophage and microglia to injured brain. (2) Lipo@GB-DHA show an excellent role in scavenging ROS so that it can effectively inhibit the apoptosis of neuron. (3) Lipo@GB-DHA protected neuron function by transferring the "pro-inflammatory" M1 microglia to "tissue-repairing" M2 microglia, inhibiting inflammation and promoting angiogenesis. (4) Lipo@GB-DHA decoyed the macrophages/neutrophils infiltration, mitigating secondary damage.

polycarbonate filters (Nuclepore^{TM}; Whatman) eleven times using a liposome extruder (HandExtruder^{TM}; Genizer). Finally, Lipo@GB-DHA was obtained. Lipo@DHA with the addition of DHA was prepared as a control using the same method.

2.5. *Characterization of Lipo@GB-DHA*

The hydrodynamic diameter and zeta potential of the liposomes were measured at 25°C using dynamic light scattering (DLS) with a Zetasizer Nano-ZS system (Malvern 3600; Malvern). A transmission electron microscope (G2 Spirite 120 kV; FEI) was used to visualize the morphology of Lipo@GB-DHA and Lipo@DHA stained with 2% uranyl acetate [32]. Finally, Lipo@GB-DHA was suspended in 1 × PBS and stored at 4°C. The diameter, polydispersity index (PDI), and zeta potential were measured.

The encapsulation efficiency (EE) of GB-DHA in liposomes was calculated by measuring the drug content in the filtrate collected by SephadexG-50 to the total added GB-DHA using HPLC (Agilent 1200) at 205 nm [33,34], A Cosmosil C18 column (5 μm, 4.6 mm × 250 mm) was used and the mobile phase consisted of a 0.1% phosphoric acid and acetonitrile (20:80, v:v). The EE was calculated using the following equation:

$$EE(\%) = W_{filtrate} / W_{total} \times 100\%$$

where $W_{filtrate}$ is the amount of GB-DHA collected by SephadexG-50, and W_{total} is the total amount of added Lipo@GB-DHA.

The release kinetics of GB-DHA from Lipo@GB-DHA was carried out by dialysis bags. 2 ml Lipo@GB-DHA containing GB-DHA (3.46 mg/ml with 2 mg/ml GB) was dispersed into dialysis bags with a molecular weight (MW) cutoff of 3.5 kDa and dialyzed in 100 ml of PBS without or with different concentrations of Tween 80 (0.1%, 0.3%; w/w). Samples in dialysis bags were taken out at specific time points and replaced with fresh buffer at the same volume [35]. The remaining amount of GB-DHA was quantified by HPLC.

2.6. Cell viability with Lipo@GB-DHA after oxygen-glucose deprivation /reperfusion (OGD/R)

Firstly, cell viability of PC12 cells treated with different formulations (GB injection, GB-DHA, Lipo@DHA, and Lipo@GB-DHA) was investigated. Typically, PC 12 cells were seeded on 96-well plates (5×10^4 cells/well) incubated with different concentrations (1.5-380 μM) of formulations containing GB or DHA for 24 h before MTT assay. The absorbance of each well was recorded at 490 nm by microplate reader (ELX800, Bio-Tek)

To study the capacity of Lpo@GB-DHA to rescue dying cells after hypoxia, an OGD/R cell model was chosen to simulate the CI/RI environment *in vitro* [36,37]. Briefly, PC12 cells and BV2 cells were two cells to simulate neuron and microglia in brain, seeded in 96-well plates (5×10^3 cells/well), respectively. Then, the cells were treated with different formulations (GB injection, GB-DHA, Lipo@DHA, Lipo@GB-DHA) at a dose of 5 μg/ml GB, followed by 12 h of OGD (5% CO_2, 1% O_2, and 94% N_2 in sugar-free DMEM) and 6 h of reperfusion. Besides, the Blank group was also set with no cells and no treatments while Sham group was set with cells and PBS treatments. Finally, cell viability was tested by the MTT assay and recorded at 490 nm by microplate reader. The Cell viability was calculated using the following equation:

$$\text{Cellviability}\ (\%) = (OD_{GB} - OD_{Blank})/(OD_{Sham} - OD_{Blank}) \times 100\%$$

where OD_{GB} is the optical density of cells treated with different formulations, OD_{Blank} is the optical density of the blank plate, and OD_{Sham} is the optical density of the cells treated with PBS.

2.7. ROS assessment in vitro

The ability of Lipo@GB-DHA to resist ROS after OGD/R was evaluated using an ROS detection cell-based assay kit containing DCFDA. DCFDA can cross the cell membrane and be cleaved into DCFH by intracellular esterase, and then non-fluorescent DCFH is oxidized into highly fluorescent DCF (Ex/Em = 488 nm/525 nm) by excess ROS [38]. Briefly, PC12 cells were seeded at a density of 2×10^5 cells per well in 12-well plates and cultured for 12 h. Then, the cells were incubated with GB injection, GB-DHA, Lipo@DHA, and Lipo@GB-DHA (containing 5 μg/ml GB) for another 12 h, followed by OGD (5% CO_2, 1% O_2, and 94% N_2 in sugar-free DMEM) for 6 h, and reperfusion for 2 h. After rinsing twice with PBS, the cells were co-cultured with 10 μM DCFH-DA for 20 min in HBSS. The fluorescence of DCF was visualized using an inverted fluorescence microscope (Olympus ix73; Olympus) or quantified using flow cytometry (Cytoflex S; Beckman) at 525 nm.

2.8. Apoptosis assessment in vitro

To determine the inhibition effect of Lipo@GB-DHA on cell apoptosis after OGD/R, an Annexin V-FITC/PI (propidium iodide) apoptosis detection kit was used to evaluate cell apoptosis after OGD/R and different treatment. Briefly, PC12 cells pre-treated with different formulations were cultured in 6-well plates for 12 h and collected after 6 h of OGD and 2 h of reperfusion. The cells were collected by centrifuge and rinsed with PBS twice, furtherly stained with 5 μl Annexin V-FITC for 10 min, followed by 5 μl PI co-incubation for another 5 min on ice. Finally, the cells were analyzed using flow cytometry (Cytoflex S; Beckman) at 488/560 nm.

2.9. Microglial phenotype assessment in vitro

To evaluate the effect of Lipo@GB-DHA on the microglial phenotype, primary microglia were isolated from newborn rats according to a previously published method [39,40]. Specifically, the cortex of P2 rats was separated from the whole brain and placed in 1640 culture medium, whereas the meninges were abolished. The tissue samples were blown repeatedly with a pipette and centrifuged at 400 $\times$ *g* for 5 min. The resulting supernatant was discarded and 0.125% trypsin was added to centrifuge tube for 15 min digestion at 37°C. The digested samples were filtered through a 70-mesh sterile filter and transferred to DMEM culture medium containing penicillin-streptomycin and 10% FBS. Finally, the cells were collected and plated into PDL(Poly-D-lysine)-coated T-75 flasks with 15 ml DMEM culture medium and stored in a cell culture incubator with 5%CO_2 and 100% humidity at 37°C. When a cell layer was nearly complete, microglia were collected by collecting supernatant after shaking flasks at 180 rpm for 2 h at 37°C and then plated in culture medium to achieve a density of 5×10^5 cells/ml.

Flow cytometry and immunofluorescence staining were used to quantify the primary microglial phenotypes. Briefly, primary microglia were seed on 24-well plate overnight and then co-incubate with Lipo@GB-DHA for 12 h before 6 h of OGD and 2 h of reperfusion. Furtherly, primary microglia was stained with PE anti-rat CD86 (1:250) (14-0081-82; eBioscience) and APC anti-rat CD206 (1:250) (201805; Santa Cruz) at room temperature for 30 min, and then analyzed by flow cytometry (Cytoflex S; Beckman) at 560 nm/647 nm. For the immunofluorescence staining assay, M1 phenotypic marker CD86 (1:800) (E2G8P; CST) and M2 phenotypic marker CD206 (1:400) (ab64693; Abcam) were visualized using an inverted fluorescence microscope (Olympus ix 73; Olympus) and quantified using Image J software.

2.10. Inflammatory cytokines tests by RT-qPCR in vitro

Microglia are immune sentinels capable of orchestrating a potent inflammatory response in the central nervous system (CNS). To evaluate the cytokines in microglia after OGD/R, RT-qPCR was used to analyze the gene expression of inflammatory-related cytokines, as described previously [41]. BV2 cells were treated with 6 h of OGD and 2 h of reoxygenated after 12 h of Lipo@GB-DHA pretreatment (GB normalized to 5 μg/ml). Total RNA was extracted from BV-2 cells using TRIzol (19201ES60; Yeasen) according to the manufacturer's instructions, as previously reported [42]. Next, 1.0 μg of total RNA was reverse-transcribed to cDNA using a PCR system (C1000; Bio-Rad) and RT-qPCR analysis was performed on a Real-Time PCR System (ABI QuantStudio 3; AB) with Hieff® qPCR SYBR Green Master Mix (Low Rox Plus) (11202ES03; Yeasen). The CT values were used to analyze qPCR data using GADPH as an endogenous reference in each sample. The

primers used in this study are listed in Table S3. And the gene expression evaluation *in vivo* was also carried out with the primers in Table S4.

2.11. Establishment of middle cerebral artery occlusion model (MCAO) of rats

Male SD rats (weighing ~250 g) were subjected to MCAO using the suture method, according to previous reports [43,44]. Briefly, the rats were anesthetized with 2% sodium pentobarbital, and the left common carotid artery (CCA), external carotid artery (ECA), and internal carotid artery (ICA) of the rats were exposed. A small incision was carefully made at the ECA, and a nylon suture was inserted from the incision and turned into the ICA. The depth of the suture insertion was kept at 18 mm. The suture was withdrawn after 1.5 h to achieve reperfusion. Throughout the operation, body temperature was maintained at 37 ± 0.5°C by placing the rats on a heating pad.

2.12. In vivo imaging of Lipo@GB-DHA in the rat brain

The whole-body NIR fluorescence imaging system (Cailper; PerkinElmer) was used to evaluate the distribution of Lipo@GB-DHA *in vivo* and *ex vivo*, as previously reported [43]. While free DID was used as a control by dispersing DID in a 0.5% Tween 80 solution. As reported, 1% Tween 80 will help Graphene oxide (GO) lower distribute in lung but more in liver, but no alternation in other organs including brain was found with or without Tween 80 [45]. So, a buffer containing 0.5% Tween 80 may not affect the distribution in brains. After 2 h of reperfusion, MCAO rats (220-250 g) were intravenously injected with DID-labeled Lipo@GB-DHA (or free DID) at a dose of 200 μg/kg DID, and *in vivo* fluorescence images were captured at 0.5, 1, 2, 4, 6, 12, 24 h. At 24 h post-injection, the brains were isolated from rats for *ex vivo* imaging, and the main organs (heart, liver, spleen, lung, and kidney) were also collected to observe the biodistribution of Lipo@GB-DHA in MCAO rats. The results were analyzed using Living Image software (version 4.3).

To assess the target cell of Lipo@GB-DHA in the brain, immunofluorescence staining was performed, as previously reported [46]. At 24 h post-injection, the rats were sacrificed and the brains were collected and fixed with paraformaldehyde (4%) for further frozen sections. The sections were labeled with Iba-1 (1:400) (GB12105; Servicebio) and GFAP (1:800) (ab7260; Abcam), followed by incubation with immunofluorescence secondary antibodies. The sections were visualized using a rotary confocal microscope (SR10; Olympus) at 405/488/560/647 nm. The colocalization of DID with different cells was analyzed using ImageJ software.

2.13. Anti-ischemic stroke efficacy of Lipo@GB-DHA with different dosing time

To determine how therapeutic time windows affect outcomes, TTC (2,3,5-triphenyltetrazolium chloride) staining was conducted at the end of two experiments with different dosing times [47,48]. At 2 h of reperfusion, GB injection, Lipo@DHA, and Lipo@GB-DHA were administered by intravenous injection at a dose of 5 mg/kg GB. The Sham and MCAO groups were administered PBS. Then, 24 h after reperfusion, the brains of MCAO rats were collected, and the infarct volume was assessed by TTC staining. In another experiment, GB injection and Lipo@GB-DHA were administered at a dose of 5 mg/kg GB at 6 h after reperfusion to simulate untimely clinical treatment. Rat brains were collected 72 h after injection. Then, coronal sections (2 mm-thick) of the brain tissue were stained with 2% TTC. ImageJ was used to calculate the infarct area without red staining. The total infarct volume (%) was determined as the ratio of the total infarct volume to the ischemic hemisphere volume and modified neurological severity score (mNSS) (score 0, no damage; score 18, severe damage) [44] were collected in each group.

2.14. Anti-ischemic stroke efficacy of Lipo@GB-DHA with multi-dose treatment

MCAO rats were injected with GB, Lipo@DHA, and Lipo@GB-DHA after 6 h of reperfusion on Day 0, 3 and 6 at a dose of 5 mg/kg GB. Every three days, the body weight and mNSS scores were collected in each group. Furthermore, to monitor brain edema during the dosing process, MRI was performed on the first and seventh days after MCAO, as previously described [49]. Briefly, the treated rats were anesthetized with 2% pentobarbital sodium via intraperitoneal injection and placed in an MRI machine with a specific rat holder. MRI scanning was conducted using a T2W sequence on a 3.0 T spectrometer (GE Prisma). The collected data were viewed by a Radiant Dicom viewer, and the shaded lesions were quantified using ImageJ. Edema area was determined using the following equation:

$$\text{Edemaarea}\ (\%) = (A2/A1) \times 100\%$$

where A1 is the area of the intact regions of the ipsilateral (left) hemisphere and A2 is the area of the shaded lesion in the left hemisphere.

2.15. Brain immune cells analysis

Flow cytometry is an efficient technique for assessing the expression of several markers and distinguishing cell populations in the brain, as previously described [50–52]. Briefly, the rat brains were sectioned using small scissors for dispersion. The suspension was then passed through a nylon mesh (70-μm pore size; Millipore) in a 50 ml tube using a syringe plunger. Then, the suspensions were dispersed in PBS and placed carefully on 30% and 70% Percoll gradients (P4937; GE). The gradients were centrifuged at 1,500 × *g* for 20 min at room temperature to remove medulla and red blood cells, respectively. The cells between 30% and 70% Percoll gradients were collected and blocked with 1% FBS, followed by staining with fluorescent antibodies. To analyze macrophages and microglia, cells were stained with Alexa Fluor®700 anti-rat CD45 antibody (1:300) (202218; BioLegend), FITC anti-rat CD11b/c antibody (1:500) (201805; BioLegend), PE anti-rat CD86 (1:250) (14-0081-82; eBioscience), and APC anti-rat CD206 (1:250) (201805; Santa Cruz). To analyze lymphocytes,

brain cells were stained with Alexa Fluor®700 anti-rat CD45 antibody (1:300) (202218; BioLegend) and FITC anti-rat CD3 (1:500) (201403; BioLegend). The stained cells were detected using flow cytometry (Cytoflex S; Beckman) and analyzed using FlowJo software.

To assess the neuroprotective effect of Lipo@GB-DHA on brain cells, TUNEL staining was carried out. The treated rats were anesthetized and sacrificed after 14 d of treatment. Brain tissue sections were fixed in paraformaldehyde (4%), followed by permeabilization with Triton X-100 solution (0.1%), and blocked with bovine serum albumin (5%) for 1 h. Then, the brain sections were co-incubated with antibodies NeuN (1:400) (GB11138; Servicebio), and then stained with One-Step TUNEL Apoptosis Assay Kit (G1501-50T; Servicebio) according to the manufacturer's instructions. In addition, to determine the effect of Lipo@GB-DHA on the microglial phenotype in the brain, Iba-1 (1:400) (GB12105; Servicebio) and CD206 (1:400) (GB113497; Servicebio) were used to label microglia and the M2 phenotype, respectively. The above sections were visualized using a spinning disk confocal super-resolution microscope (SR10; Olympus).

2.16. *Western blotting analysis*

Western blotting was used to evaluate protein expression in the ischemic hemisphere. Protein samples were isolated by homogenization and then centrifuged at 4 °C at 12,000 × *g*, as described previously [53]. Brain lysate was centrifuged at 4°C for 20 min at 12,000 × *g* and the total concentration of protein was quantitated by BCA protein assay kit (Omni-Easy^{TM}; Easy^{TM}). Samples with the concentration of 2 mg/mL protein were denatured at 90°C for 10 min. Next, 40 μg protein was separated by sodium dodecyl sulfate-polyacrylamide gel electrophoresis (SDS-PAGE), followed by transfer to 0.45 μm nitrocellulose membranes (Millipore, USA). The membranes were blocked with 5% BSA in Tween-20/TBS buffer for 1 h and then incubated with primary antibodies overnight related to apoptosis, including rabbit anti-BDNF (1:2000) (ab226843; Abcam), rabbit anti-Bcl-2 (1:2000) (ab182858; Abcam), rabbit anti-Bax (1:2000) (ab32503; Abcam), rabbit anti-caspase 3 (1:1000) (A19664; Abclonal), and rabbit anti-β-actin (1:1000) (GB11001; Servicebio). The following antibodies were used: rabbit anti-LC3B (1:1000) (A19665; Abclonal), rabbit anti-p-AMPK (1:1000) (A1229; Abclonal), rabbit anti-p-TAK1 (1:1000) (AP0071; Abclonal), rabbit anti-ATG5 (1:1000) (AF2269; Beyotime), and rabbit anti-β-actin (1:1000) (GB15001; Servicebio). Horseradish peroxidase (HRP)-conjugated secondary antibodies (1:3000) (30403ES40; Yeason) were used to replace the primary antibodies, and the membranes were visualized using an imaging system (Bio-Rad, USA) with enhanced chemiluminescence.

2.17. *Safety evaluation* in vivo

After multiple administration experiments, the safety of the preparation was assessed by measuring the concentrations of serum creatinine (CREA) and blood urea nitrogen (UREA) in serum. Hematoxylin and eosin (H&E) staining was performed by pathologists to visualize cellular and tissue structure details.

2.18. *Statistical analysis*

GraphPad Prism (version 8.0) was utilized for statistical analysis. The two-tailed student's t-test was applied to assess the differences in means between two groups. One-way ANOVA was employed to detect differences among three or more groups. Two-way ANOVA was used to determine the differences in means across three or more groups over time.

3. Results and discussion

3.1. *Synthesis of GB-DHA complex*

Considering the limited druggability and treatment efficiency of GB, a complex strategy was proposed by reforming GB and DHA, which act as ROS scavengers with a long-chain fatty acid structure [54]. The synthetic procedure for GB-DHA is illustrated in Fig. S1A, which involved the esterification of the 10-hydroxyl group of GB and the carboxyl group of DHA. The double linkage of DHA (5-6 ppm) and the methyl group of GB (0.5-1.5 ppm) were clearly observed in the ^{1}H-NMR spectrum (Fig. S1B). The molecular ion peaks of GB-DHA visible in the electrospray ionization mass spectrometry (ESI-MS) spectrum were [M+1] = 735 and [M+23] = 757. And the ratio of conjugated GB and DHA was 1:1. Furthermore, the addition of DHA significantly improved the lipophilicity of GB, and the calculated LogP value was 5.8 ± 0.13, which was significantly higher than that of GB, as previously reported [17].

3.2. *Preparation and characterization of Lipo@GB-DHA*

Liposomes containing the GB-DHA complex were fabricated using a thin-film hydration technique (Fig. 1A). The EE was optimized by selection of GB-DHA/egg yolk lecithin (EPC) fed ratio (Table S1). Under the same condition, the highest EE was up to 91.8% when the optimized weight ratio of GB-DHA to EPC was 1:15. Furthermore, when the ratios of cholesterol to phospholipids were in the range of 10:2-10:3, the PDI of liposomes was less than 0.3 (Table S2). These results were consistent with the previously report that a higher cholesterol ratio could increase liposome stability by modulating phospholipid packing [55]. However, considering that a high level of cholesterol is associated with an increased risk of ischemic stroke [56], a phospholipid to cholesterol ratio of 10:2 may be a better choice. Ultimately, the final liposome was consisted of 1.73 mg/ml GB-DHA (containing 1 mg/ml GB), 15 mg/ml EPC, 3 mg/ml cholesterol, and 1.5 mg/ml DSPE-PEG_{2000}.

Furtherly, the Lipo@GB-DHA and control Lipo@DHA were characterized (Fig. 1B-1D). The average diameter of Lipo@GB-DHA measured by dynamic light scattering (DLS) was 109.3 ± 1.68 nm (Fig. 1B), while the PDI was 0.179 ± 0.02, which indicated Lipo@GB-DHA had narrow size distribution value. The ζ-potential of Lipo@GB-DHA dispersed in deionized water was –32.0 ± 1.51 mV (Fig. 1D), giving an indication of the potential stability of nanomedicine [57]. The morphology of Lipo@GB-DHA, characterized by transmission electron microscopy (TEM), showed a homogenous spherical shape (Fig. 1C). The diameter of control group Lipo@DHA was 102.8

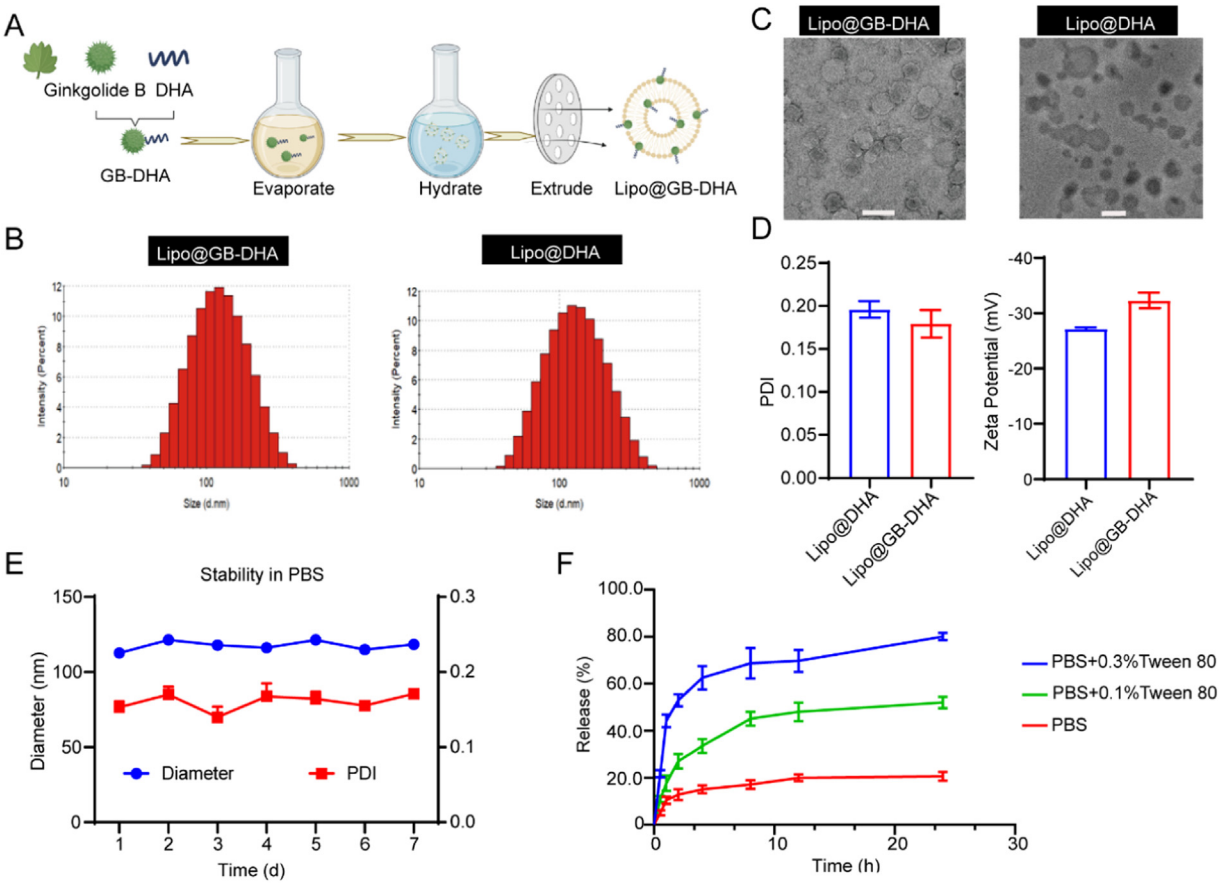

Fig. 1 – Schematic illustration of the fabrication and characterization of the Lipo@GB-DHA. (A) Schematic diagram of the preparation of Lipo@GB-DHA. (B-C) DLS (B) and TEM (C) analysis of Lipo@GB-DHA and Lipo@DHA (Scale bar: 200 nm). (D) PDI and zeta potential of Lipo@DHA and Lipo@GB-DHA. (E) The diameter and PDI stability of the Lipo@GB-DHA in 1 × PBS for 7 days at 4 °C (n = 3). (F) Drug release kinetics of the Lipo@GB-DHA in 1 × PBS, 0.1% Tween 80 + 1 × PBS, and 0.3% Tween 80 + 1 × PBS *in vitro* (n = 3). Data are presented as the means ± SD.

± 1.1 nm (PDI = 0.196 ± 0.03), showing a black spherical shape may attribute to the hydrogen bonding between uranyl acetate and the carboxyl group of DHA (Fig. 1B-1D) [58].

To study the stability of Lipo@GB-DHA in 1 × PBS (pH 7.4), its diameter and PDI were recorded. The diameter of Lipo@GB-DHA was stable in the nanosized range, with a low value of PDI for 7 days at 4 °C (Fig. 1E). A high stability is beneficial for preservation in the liquid state. To investigate the drug release capacity of Lipo@GB-DHA, the release behavior of GB-DHA was analyzed by dialyzing against PBS (pH 7.4) containing different concentrations of Tween 80 (0%, 0.1% and 0.3%, w/w) at 37°C. Approximately 20.6% of GB-DHA was released in PBS, while nearly 52.0% GB-DHA was released in 0.1% Tween 80 and 80.2% in 0.3% Tween 80 after 24 h (Fig. 1F). Here, a low release rate in PBS indicates that GB-DHA has good compatibility with the lipid bilayers and is more stable in the systemic circulation.

3.3. *Neuroprotection effect of Lipo@GB-DHA via ROS scavening* in vitro

To clarify the mechanisms of neuroprotection, oxidative stress caused by blood-flow-deprived and sudden brain reoxygenation was investigated *in vitro* [59]. In this study, oxidative free radicals in PC12 cells after reoxygenation were quantified using DCFDA (Fig. 2A-2B). intracellular DCFDA fluorescence in the OGD/R group was significantly enhanced up to 2.1 times that of the Sham group, meaning a successful *in vitro* anoxia-reoxygenation cell model was constructed. The significantly lower fluorescence of DCFDA in the Lipo@GB-DHA group than in the GB injection group indicates that DHA plays a vital role in ROS scavenging due to its enhanced mitochondrial function and biogenesis capability, as reported [27]. In addition, the fluorescence intensity in Lipo@GB-DHA group was reduced to 0.6 times that in the GB-DHA group, the phenomenon may attribute to that Lipo@GB-DHA could be better uptake by cells. Here, the above results indicated that Lipo@GB-DHA show neuroprotective functions via scavenging ROS to block subsequent damage.

Before studying cell viability, the cytotoxicity of various formulations in PC12 cells was examined by MTT assays. After 24 h of co-incubation, the IC_{50} values for GB-DHA, Lipo@DHA, and Lipo@GB-DHA were 130.9, 167.6 and 162.4 μM (Fig. S2), respectively, meaning that the encapsulation of liposomes slightly reduces the cytotoxicity. Besides, the results also

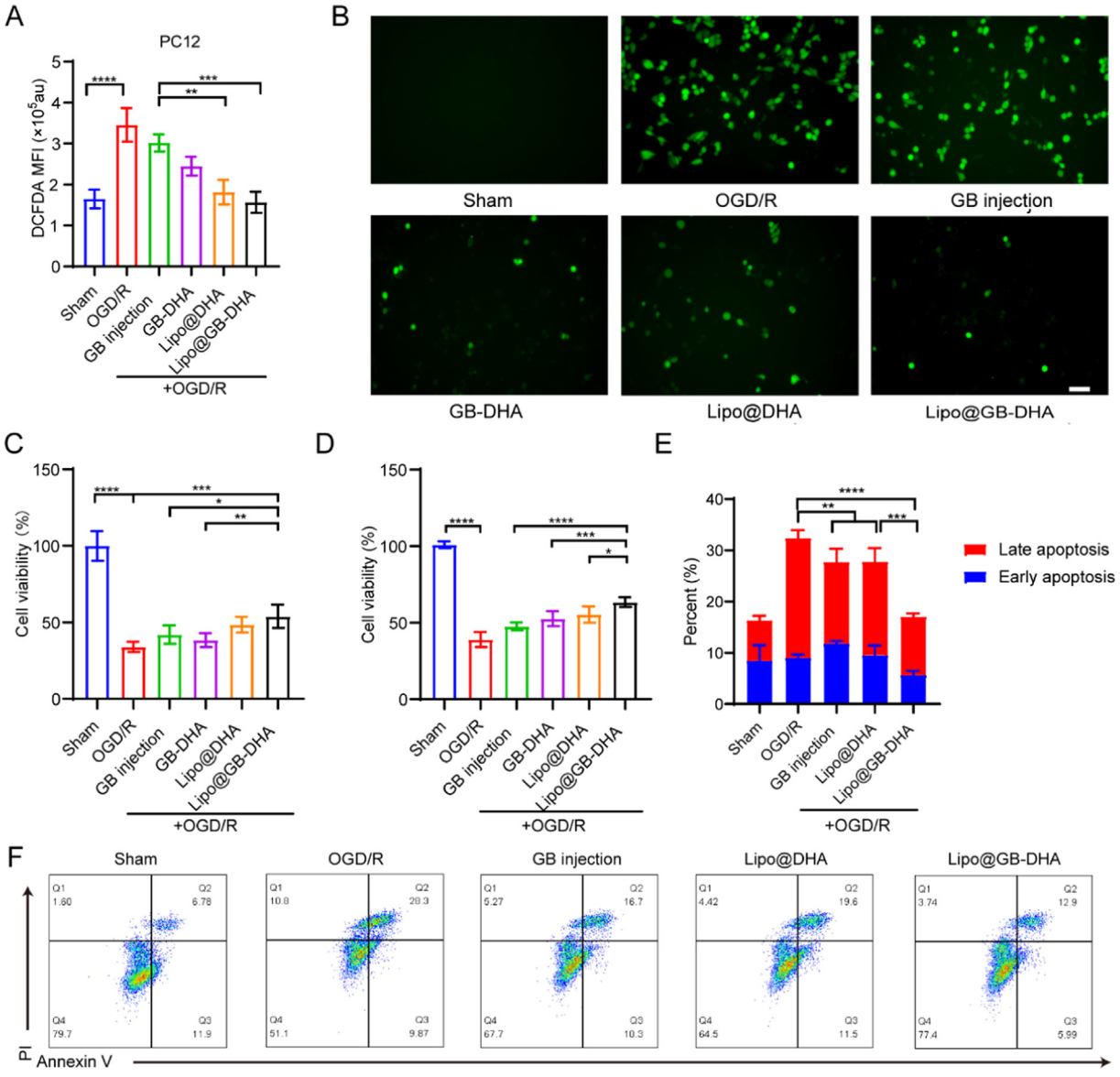

Fig. 2 – Anti-apoptosis capacity of Lipo@GB-DHA via ROS scavenging *in vitro*. (A-B) Quantification (A) and representative fluorescence images (B) of DCFDA revealed relative intracellular ROS levels after OGD/R (Scale bar: 50 μm). (C-D) Cell viabilities of PC12 cells and BV2 cells with Lipo@GB-DHA for 12 h, followed by 12 h of OGD and 2 h of reperfusion ($n = 6$). (E-F) Representative flow cytometric images and quantitative data of cell apoptosis tested by Annexin V-FITC/PI staining after OGD/R ($n = 4$). Data are presented as the means ± SD; *P < 0.05, **P < 0.01, ***P < 0.001.

indicated that 5 μg/ml (~11.8 μM) of GB in liposomes did not affect cell survival after 24 h of incubation.

To furtherly elucidate the neuroprotective effects of Lipo@GB-DHA, cell viability assays were performed following OGD/R. Here, OGD/R-induced cell viability of PC12 and BV2 cells decreased to below 50.0%, respectively. After pre-treatment with Lipo@GB-DHA at a dose of 5 μg/ml GB, the highest cell viability of PC12 and BV2 increased up to 54.0% and 64.5%, respectively (Fig. 2C-2D). The lower proliferation rates of Lipo@DHA compared to Lipo@GB-DHA were confirmed to be due to the lack of GB, an indication of the neuroprotective effect of GB. These results indicate that Lipo@GB-DHA synergistically protect the cells from OGD/R-induced damage.

Furthermore, the apoptotic state of cells was studied after OGD/R [60]. After 6 h of OGD followed by 2 h of reoxygenation, significant necroptosis was observed (Fig. 2E-2F). The total apoptosis cells in OGD/R group were reduced from 32.4% to 17.3% by Lipo@GB-DHA treatment, significantly lower than 27.7% by GB injection and 27.8% by Lipo@DHA. Here, Lipo@GB-DHA could significantly down-regulate both the ratio of early apoptotic cells and late apoptotic cells, indicating that the strategy of the GB-DHA complex and liposomal encapsulation further enhanced neuroprotective efficacy. These results may

be related to the lower ROS levels in the Lipo@GB-DHA group, which play an important role in apoptosis induction [61].

3.4. *Modulating microglia M2 polarization by Lipo@GB-DHA* in vitro

Microglia are massively activated in the ischemic hemisphere and play a role in phagocytosis and the regulation of inflammation. In particular, M2 microglia secretes anti-inflammatory cytokines and acts as "restorers" of brain injury [62]. Here, to understand the regulatory ability of Lipo@GB-DHA, OGD/R was applied to primary microglia, and the cell phenotypes were monitored after different treatments (Fig. 3A-3D). OGD/R caused the overexpression of the M1 marker CD86 and the downregulation of the M2 marker CD206 in primary microglia, which indicates a fast phenotypic transition under oxidative stress. GB injection treatment downregulated the expression of the M1 marker CD86, while Lipo@GB-DHA treatment reduced the level of CD86 and enhanced the expression of the M2 marker CD206 at the same time. The results were consistent with the previous report that GB can suppresses M1 polarization via inhibiting NLRP3 inflammasome activation [63], while DHA can upregulate M2 polarization through activating p38 MAPK signaling pathway [64]. The higher ratio of M2/M1 microglia enhanced by Lipo@GB-DHA may be attributed to the coordinated modulation of GB and DHA, which may take part in the inflammatory responses caused by excessive activation of microglia after stroke.

To illustrate the effect of microglial phenotype on inflammation level, total RNA was extracted, and the gene expression of inflammatory cytokines in BV2 cell lines was evaluated by RT-qPCR. The results showed that the pro-inflammatory TNF-α, IL-1β, IL-6, CCL2, and CD86 levels increased 3.0, 6.1, 53.7, 1.5, and 2.5 times after OGD/R, respectively (Fig. 3E-3I). Upon treated with Lipo@GB-DHA, pro-inflammatory cytokines in BV2 were reduced by 64.9%, 61.4%, 38.1%, 30.0%, and 48.8%, significantly lower than those in GB injection group and Lipo@DHA group. The secretion of anti-inflammatory cytokines IL-10 in BV2 cells increased to 1.52 and 1.73 times after co-culturing with GB injection and Lipo@GB-DHA, indicating that GB may play a role in anti-inflammatory cytokines secretion (Fig. 3J). Therefore, the superiority of Lipo@GB-DHA in neuroinflammation modulation via regulating microglial phenotypes was validated. These findings confirm that Lipo@GB-DHA not only polarizes the microglial phenotype from M1 to M2 but also modulates inflammatory responses after CI/RI.

3.5. *Targeting capacity of Lipo@GB-DHA to ischemic hemisphere* in vivo

To discuss the *in vivo* biodistribution of Lipo@GB-DHA in ischemic lesions, a rat model of MCAO was carried out and the rats were injected with Free DID/Tween 80 and Lipo@GB-DHA/DID at a dose of 200 μg/kg DID, respectively. At various times after *i.v.* administration, the fluorescence intensity of Lipo@GB-DHA observed in the brains of MCAO rats was 1.8 to 7.4 times that of Free DID/Tween 80 group (Fig. 4A-4B), the results demonstrated that Lipo@GB-DHA could more accumulate in the brain than free solution. Here, a higher Free DID/Tween 80 accumulation at post-administrated may be related to inadequate lysosome escape. Briefly, after being endocytosed by caveolin, Lipo@GB-DHA will quickly enter the lysosome and can escape successfully at 8 h, however, Free DID/Tween 80 show a poor escape capacity, so that Free DID/Tween 80 may lead persistent fluorescence accumulation at 24 h (Fig. S3 and 4A).

Besides, the *ex vivo* fluorescence intensity of Lipo@GB-DHA in the ischemic hemisphere was more than that in the normal side (Fig. 4A), while approximately 2.1 times that of free DID/Tween 80 in the ischemic hemisphere (Fig. 4C). Here, Lipo@GB-DHA/DID was also demonstrated to be tend to gather in the ischemic hemisphere once after 2 h of injection (Fig. S4). These results both indicated that Lipo@GB-DHA/DID tends to accumulate in the ischemic hemisphere, meaning it could selectively target the ischemic infarct region. The phenomenon may be related to the high expression of caveolin after stroke in ischemic hemisphere, thereby increasing the endocytosis efficiency of liposomes as reported [65]. Here, BCEC cells was used as a cell model for its high expression of caveolin and pre-treated with different concentration of nystatin, which is a pharmacological blocker of caveolae-mediated endocytosis [66]. Then Lipo@GB-DHA labeled with 0.1% DID was added the cells and the uptake was tested by flow cytometry after 4 h of incubation. Here, by blocking the caveolin in a dose-dependent way, the uptake of Lipo@GB-DHA was also blocked in a dose-dependent way (Fig. S5), the results may indicate that a higher expression of caveolin may help Lipo@GB-DHA endocytosis.

Moreover, 24 h after injection, the brains were collected and stained with fluorescent antibody. Green fluorescence was co-localized with pink DID, indicating that microglia were more able to take up Lipo@GB-DHA than Free DID/Tween 80 (Fig. 4D-4E). Compared with astrocytes, Lipo@GB-DHA may also co-localize better with microglia (Fig. 4E), indicating that microglia may be the target cells for liposomes. Besides, the distribution of Free DID/Tween 80 and Lipo@GB-DHA/DID was similar in all organs except liver (Fig. S6A-S6B), meaning the similar amount of DID was given. Therefore, the prepared Lipo@GB-DHA can be gathered in the ischemic hemisphere (Fig. S7A-S7B), uptake especially by over-activated microglia and caveolin in injured brain.

3.6. *Therapeutic efficacy of Lipo@GB-DHA for CI/RI in MCAO rats*

To assess the therapeutic efficiency of Lipo@GB-DHA in rats with MCAO, we designed different regimens. GB injection (190626; Kangyuan), a clinically approved formulation for the prevention and recovery of stroke, was used as a positive control. First, MCAO rats were randomly assigned to Sham, MCAO, GB injection, Lipo@DHA, or Lipo@GB-DHA groups. In the first study, we evaluated the therapeutic effect of GB at a dose of 5 mg/kg in MCAO rats, administered 2 h after reperfusion and sacrificed at 24 h post-reperfusion. Triphenyltetrazolium chloride (TTC) staining was also used to differentiate between live and dead tissues as previously reported [67]. Lipo@GB-DHA-treated rats showed decreased modified neurological severity score (mNSS) to 6 and an

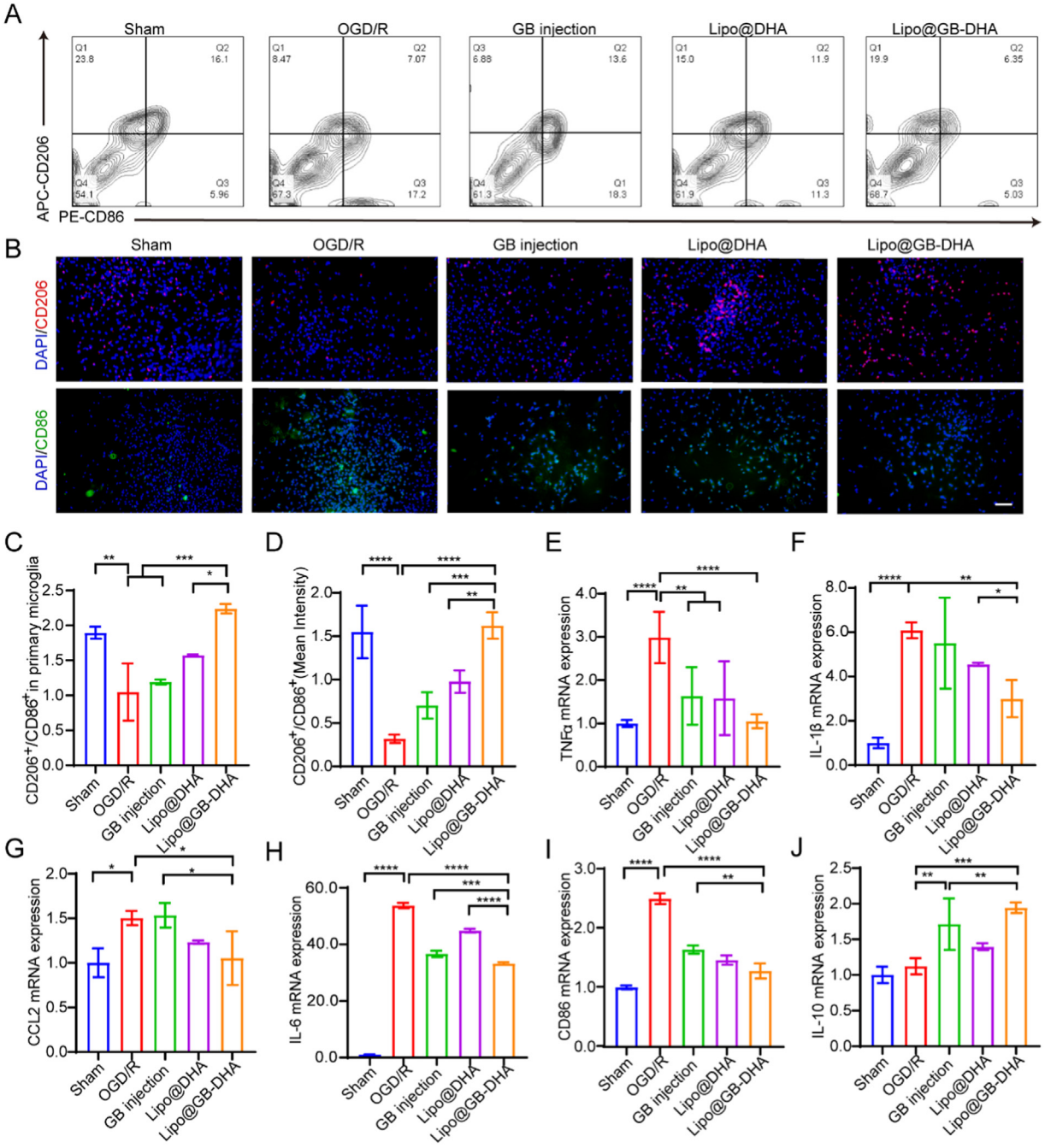

Fig. 3 – Regulation of microglia phenotypes and inflammatory cytokines secretion *in vitro*. (A-B) Representative flow cytometry images (A) and immunostaining images (B) of CD206 (M2 marker) versus CD86 (M1 marker) fluorescence in primary microglia (Scale bar: 50 μm). (C-D) Quantification of the relative fluorescence intensity of CD206 versus CD86 in primary microglia tested by flow cytometry (C) and immunostaining (D). (E–J) Gene expression of pro-inflammatory and anti-inflammatory cytokines of BV2 cells determined by RT-qPCR. Data in (C-J) are expressed as mean ± SD ($n = 6$). **$P < 0.05$,$P < 0.01$, ***$P < 0.001$, ****$P < 0.0001$.**

infarct size of 22.7% (Fig. S8A-S8C), significantly lower than GB injection-treated and Lipo@DHA-treated MCAO rats, which indicated the synergetic effects of GB and DHA. Furtherly, to investigate the therapeutic efficiency of Lipo@GB-DHA at longer dosing times, 5 mg/kg Lipo@GB-DHA was administered 6 h after reperfusion and sacrificed 72 h after reperfusion. Here, Lipo@GB-DHA-treated rats displayed a smaller infarct volume of 18.4% compared to 48.6% in MCAO rats and 41.8% in GB injection-treated rats (Fig. S8D-S8E), indicating an efficient method for CI/RI recovery no matter given at 2 h of reperfusion or 6 h of reperfusion. In previously report, GB injection showed little potential to reduce infarct volume after 6 h of reperfusion

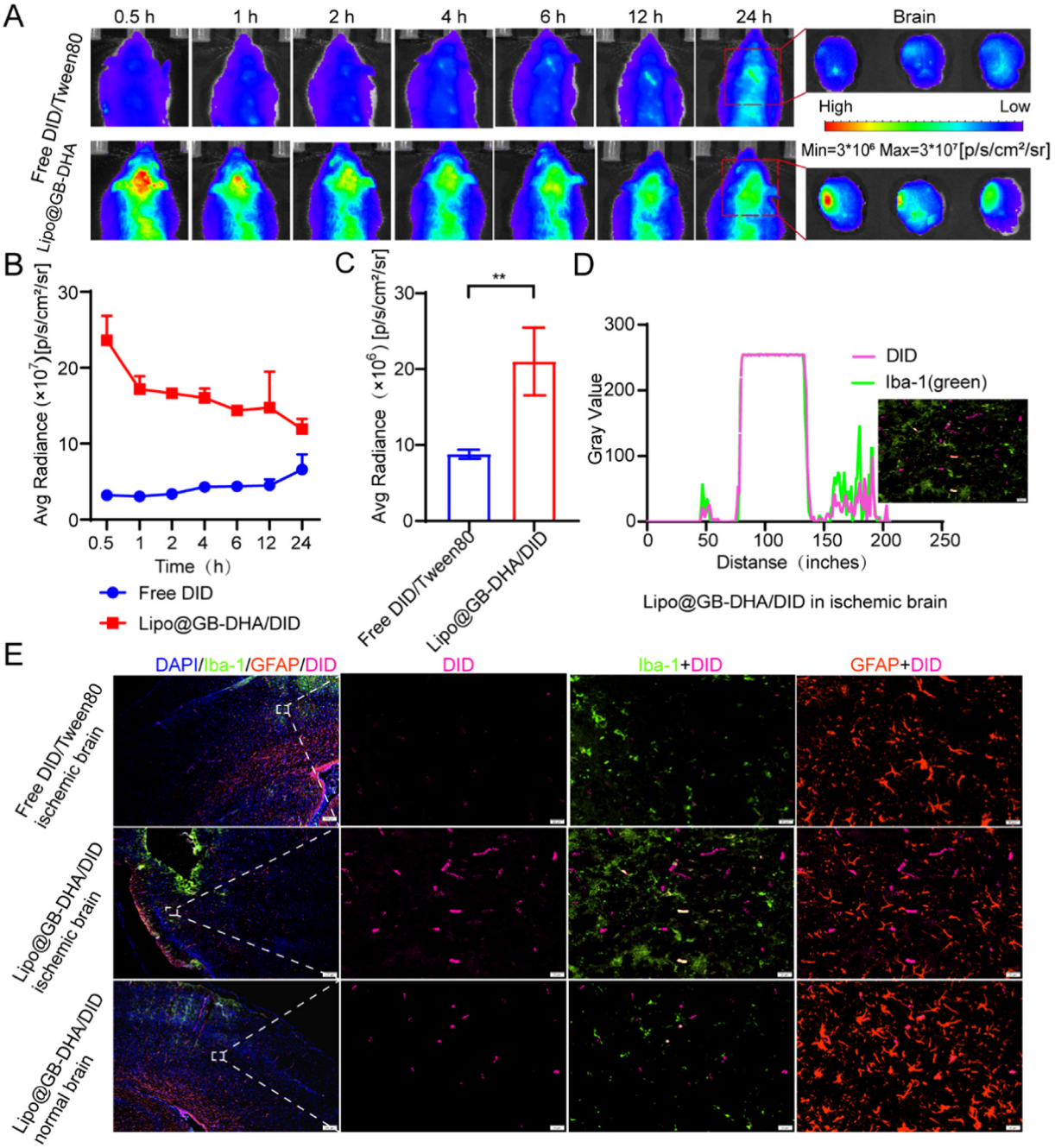

Fig. 4 – *In vivo* targeting evaluation of Lipo@GB-DHA/DiD to ischemic brain in MCAO rats. (A) *In vivo* dynamic biofluorescence imaging of brains from MCAO rat models at 0.5, 1, 2, 4, 6, 12 and 24 h post-administration after 2 h of reperfusion (left) and *ex vivo* fluorescence images of the brains at 24 h post-administration (right). (B-C) Quantified fluorescence intensity by measuring the region of interest (ROI) in *in vivo* IVIS images and *ex vivo* images ($n = 3$). (D) Co-localization of Lipo@GB-DHA/DID with microglia in brains. (E) Representative immunostaining images of Lipo@GB-DHA with microglia/astrocytes in ischemic hemisphere by Image J (Scale bar: 20/200 μm). Data in (B, C) are expressed as mean ± SD ($n = 3$). **$P < 0.01$.

[15]. So, these results may also indicate that the complex-liposome strategy has the advantage of a longer therapeutic window than the free solution on the market.

Furthermore, the therapeutic efficiency of multiple dosing was also investigated by MRI designed as Fig. 5A. Here, Lipo@GB-DHA-treated rats shown smaller encephaloedema than Lipo@DHA-treated and GB injection-treated rats at the first dose, and even no abvious white shadow remaining after all three doses (Fig. 5B). Besides, Lipo@GB-DHA-treated rats showed the best weight recovery than other postsurgical rats (Fig. 5C). And it seems that the multi-dose of Lipo@GB-DHA showed the smallest mNSS score, slightly lower than

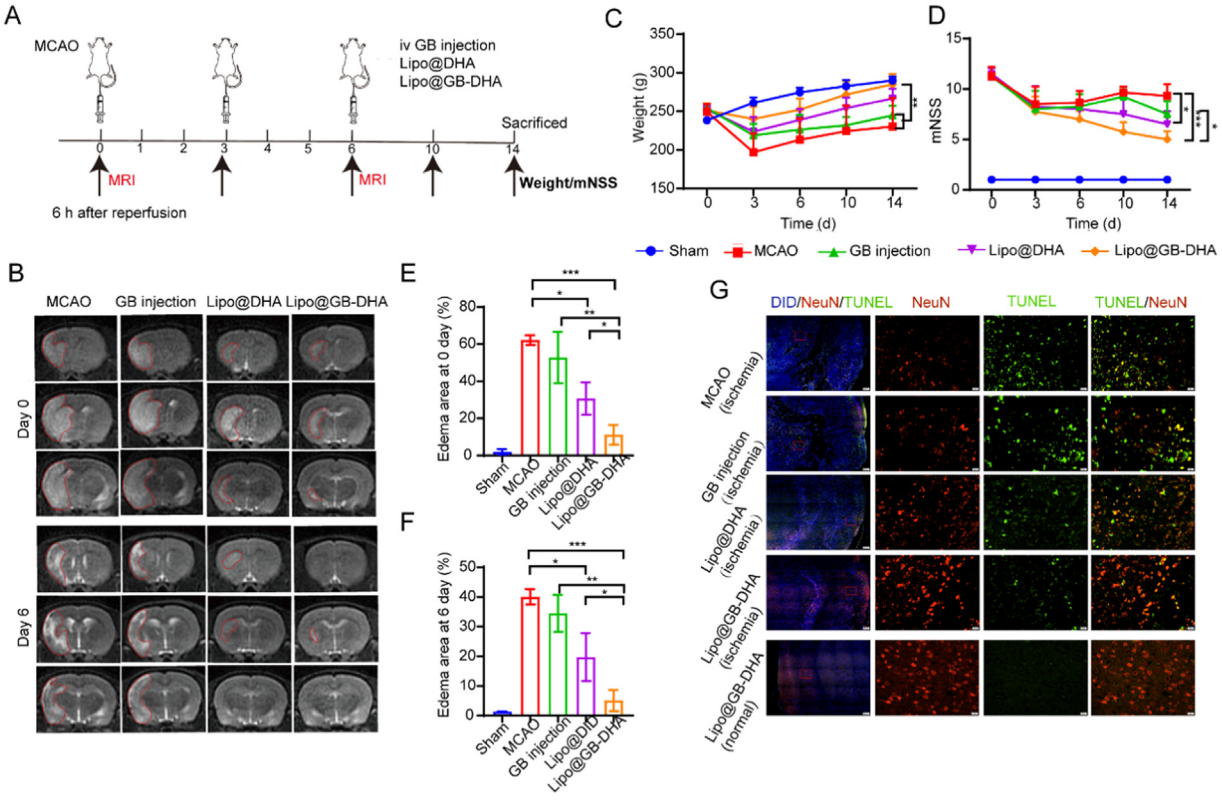

Fig. 5 – Multi-dose therapeutic efficiency of Lipo@GB-DHA in MCAO rats by i.v. Lipo@GB-DHA after 6 h of reperfusion. (A) Schematic illustration of treatment regimens. (B) Representative T2W MRI images of MCAO rats injected with different formulations at Day 0 and Day 6. (C-D) Modified neurological severity score (mNSS) and body weight of MCAO rats with different drugs during the experiment. (E-F) The quantitative data of shaded areas in brains of MCAO rats at day 0 (E) and day 6 (F). (G) Representative images of TUNEL and NeuN staining in the ischemic penumbra (Scale bars, 200 μm/20 μm). Data in (C-D, E-F) were expressed as mean ± SD (n = 4/5). *P < 0.05,P < 0.01, ***P < 0.001.**

Lipo@DHA but significantly lower than GB injection (Fig. 5D). Compared the higher mNSS score with the single-dose data in Fig. S8C and Fig. S8F, multi-dose administration of Lipo@GB-DHA was beneficial to the neurobehavioral recovery of rats. And the first dose seems vital for CI/RI recovery because Lipo@GB-DHA group showed an edema area as low as 13.4% after the first injection (Fig. 5E) while the MCAO group and GB injection group show a delayed recovery after all three doses (Fig. 5E-5F). Besides, the MRI results were also consistent with the TUNEL immunostaining results that the Lipo@GB-DHA group showed the minimal brain damage with the most $NeuN^+$ cells and the least $TUNEL^+$ cells on the ischemic side compared to the other groups (Fig. 5G). The results mean that Lipo@GB-DHA also showed enhanced therapeutic efficacy in multi-dose treatment for CI/RI, indicating the combined neuroprotective effects of GB and DHA, and the superiority of liposomes in crossing the BBB after stroke.

These findings demonstrated the significant benefits of GB injection when administered 2 h after the start of MCAO reperfusion occlusion (and a less-significant benefit when administered 6 h later), which is consistent with the literature [15,68]. In contrast, Lipo@GB-DHA showed potential in CI/RI recovery no matter administrated at 2 h or 6 h of reperfusion, which may be of great significance for patients those who receive clinical treatment untimely.

3.7. *The neuroprotection mechanisms of Lipo@GB-DHA by inhibiting apoptosis* in vivo

To verify the neuroprotective effect of Lipo@GB-DHA, H&E staining was used to assess cell morphology in the brain. The staining results showed that the morphology of the cells was noticeable changed, with a reduced cell volume and shrunken nuclei after hypoxia/reperfusion. The injured brain areas were alleviated after the administration of different formulations, especially Lipo@GB-DHA, indicating cells in the ischemic hemisphere nearly returned to a normal shape (Fig. 6A).

Therefore, we inferred that these changes may interfere with cellular crosstalk and lead to systemic changes in the ischemic brain microenvironment. The apoptotic pathway was demonstrated to participate in the neuroprotective effect of Lipo@GB-DHA in MCAO rats. A higher level of brain derived neurotrophic factor (BNDF), which can stimulate neuronal growth via the Wnt/β-catenin pathway, was observed in brains of Lipo@GB-DHA-treated rats [69]. The result suggested that Lipo@GB-DHA can stimulate neuronal growth and angiogenesis. Moreover, higher anti-apoptotic Bcl-2 protein and lower apoptotic-related proteins Bax and caspase 3 (including pro-caspase 3 and cleaved caspase 3) were expressed in ischemic hemisphere of Lipo@GB-DHA-treated

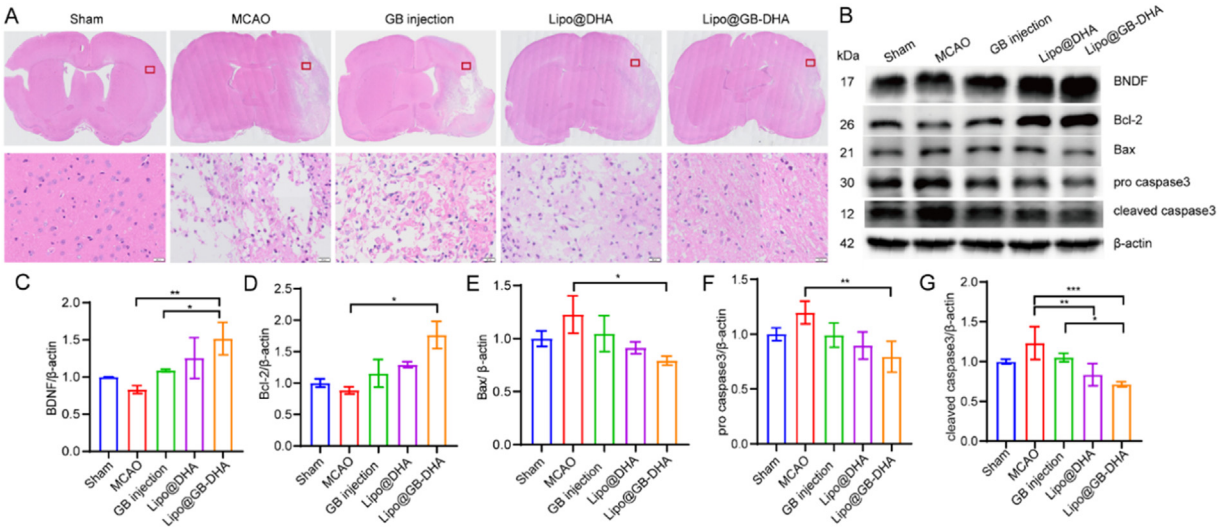

Fig. 6 – *In vivo* anti-apoptosis mechanism of Lipo@GB-DHA. (A) H&E staining of the brains from each group (scale bars: 20 μm). (B) Western blot analysis of apoptosis-related proteins in brains of MCAO rats. (C-G) Relative expression of BNDF (C), Bcl-2 (D), Bax (E), pro caspase-3 (F) and cleaved caspase3 (G) in the peri-infarct region of the brains at 14 days post reperfusion (n = 3). Data in (C-G) were expressed as mean ± SD (n = 3). *P < 0.05, **P < 0.01, ***P < 0.001.

rats (Fig. 6B-6G). The apoptotic-protein expression results also mean that Lipo@GB-DHA can inhibit the apoptotic pathway substantially protect neuron from damage.

3.8. *Immunoregulation effect of Lipo@GB-DHA* in vivo

The microglial modulatory and anti-inflammatory functions of Lipo@GB-DHA, with positive effects on different cells, have been verified in *in vitro* studies. We inferred that the positive results *in vivo* may interfere with the systemic changes in the ischemic brain microenvironment. Therefore, immune cells infiltration, inflammatory cytokines expression and autophagy activation in brains of MCAO rats were further evaluated in multi-dose experiments.

First, microglia and macrophages play vital roles in neuroinflammation after stroke. Here, $CD11b^{+}CD45^{+med}$ and $CD11b^{+}CD45^{+\,high}$ were used to label microglia and macrophages in flow cytometry, respectively [70]. With the increased permeability of the BBB after stroke, microglia were activated, while macrophages and $CD3^{+}$-labeled T cells were significantly accumulated in the brains of MCAO rats. Compared to MCAO group, macrophages, microglia, and lymphocytes were reduced to 13.8%, 46.6% and 35.9%, respectively, with Lipo@GB-DHA treatment (Fig. 7A-7E). So, the result means that Lipo@GB-DHA suppress the infiltration of peripheral immune cells to the greatest extent, compared to other treatment in this paper. Previous studies have reported that excessive peripheral immune cell infiltration exacerbates secondary brain injury [71]. Therefore, Lipo@GB-DHA can alleviate brain injury by inhibiting peripheral immune cell infiltration and the excessive activation of microglia, thus reducing secondary neuronal damage, was furtherly validated.

Furthermore, to explore other effects of Lipo@GB-DHA on microglial functions, such as polarization and phagocytosis *in vivo*, we labeled M1 microglia with CD86 antibody and M2 phenotype with CD206 antibody. The flow cytometry results showed that Lipo@GB-DHA treatment promoted the transition of microglia from M1 to M2 type *in vivo*. Among them, GB injection decreased the proportion of the M1 type, while DHA increased the proportion of the M2 type (Fig. 7E-7F), which is consistent with *in vitro* results (Fig. 3A-3D) and the immunofluorescence staining results *in vivo*, presented as an increased ratio of $CD206^{+}$ cells and a reduced number of Iba^{+}-labeled microglia (Fig. 7I). So, microglia M2 polarization was furtherly *in vivo* by Lipo@GB-DHA.

RT-qPCR was used to measure the gene expression of pro-inflammatory, anti-inflammatory, and coagulation-related cytokines in the ischemic hemisphere. The results showed that the levels of pro-inflammatory TNFα, CD86, and IL-1β increased 1.7, 13.1, and 2.7 times after MCAO. After treatment with Lipo@GB-DHA, pro-inflammatory can reduced by 78.2%, 83.1% and 60.8%, while anti-inflammatory IL-10 increased to 2.3 times and Arg1 increased to 2.4 times, compared to the MCAO group (Fig. S9A-S9E). The decreased gene expression of pro-inflammatory cytokines was consistent to *in vitro* results. Here, IL-10 was reported to possibly promote tissue regeneration in a number of ways, for example, play a role in enhancing VEGF and CXCL12 levels, and wound neovascularization, and ultimately improving cutaneous wound healing via STAT3 signaling pathway [72]. Besides, IL10/STAT3 signaling was reported to take part in alternative macrophage activation to a tissue repair phenotype, both above indicating that Lipo@GB-DHA may promote angiogenesis via up-regulating the expression of IL-10 [73,74]. What's more, PAFR and Alox12, which is

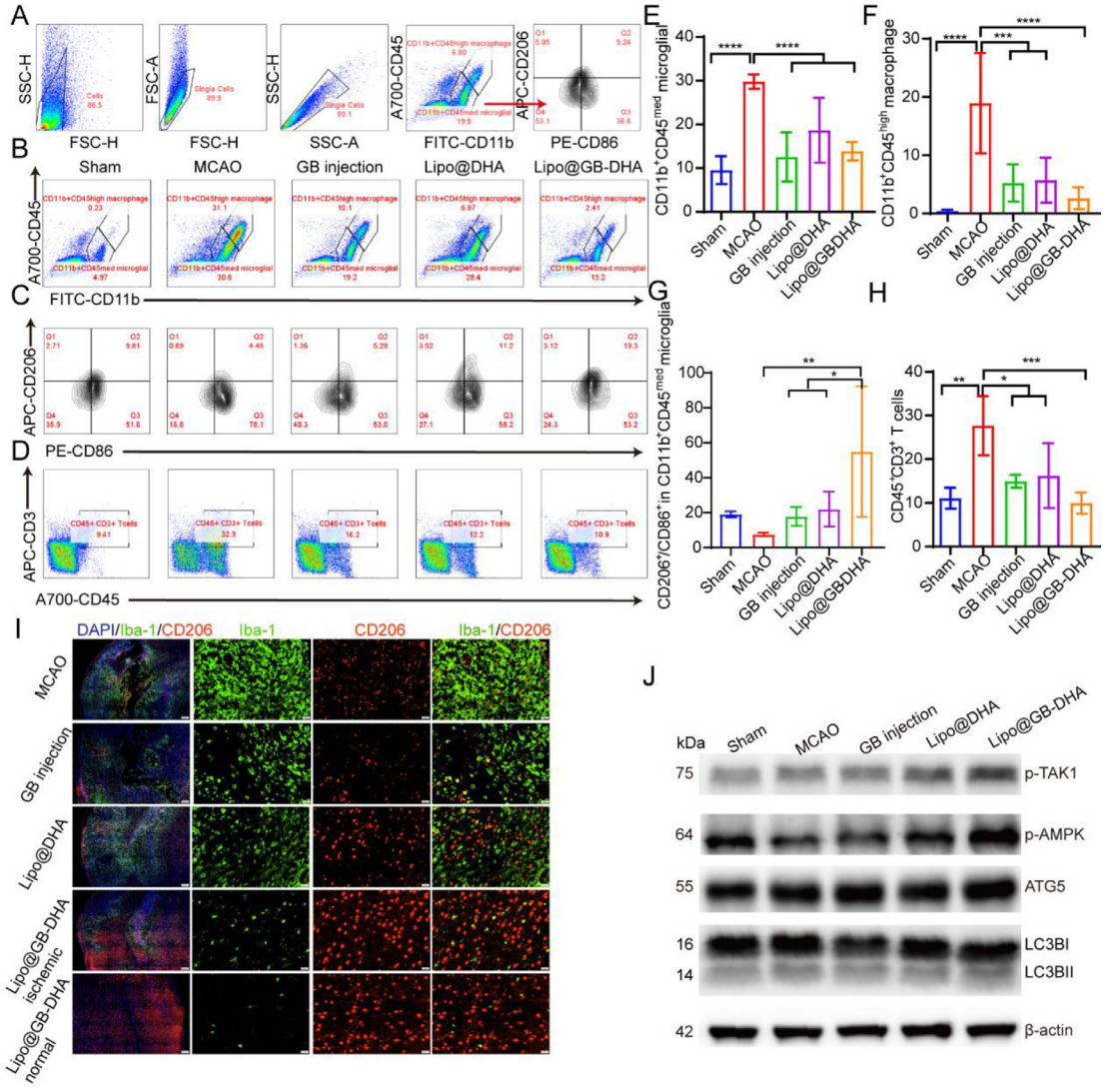

Fig. 7 – Study on remodeling of Lipo@GB-DHA *in vivo*. (A) Gating strategy of flow cytometry analysis for macrophages and microglia in brains. (B-D) Representative flow cytometry images (B) and quantifications (C-D) of $CD11b^{+}CD45^{high}$ macrophage and $CD11b^{+}CD45^{med}$ microglia in brains ($n = 6$). (E-F) Representative flow cytometry image (E) and quantifications (F) of M1/M2 cells in $CD11b^{+}CD45^{med}$ microglia in the ipsilateral side ($n = 6$). (G-H) Representative flow cytometry images (G) and quantification (H) of the proportion of $CD3^{+}$ lymphocytes in the ipsilateral side ($n = 6$). (I) Immunostaining of CD206 and Iba-1 to determine the microglial phenotype in the ischemic penumbra treated with different formulations (Scale bar: 200 μm/20 μm). (J) Western blot analysis of autophagy-related proteins in brains. Data in (D-E, F-H) were expressed as mean ± SD (n = 3). *P < 0.05, **P < 0.01, ****P < 0.0001.

associated with platelet aggregation and pro-inflammatory cytokines secretion induced by 12-hydroxyeicosatetraenoic acid (12-HETE), was keep in low level by Lipo@GB-DHA (Fig. S10F-S10G) [75,76]. Therefore, Lipo@GB-DHA can modulate neuroinflammation via multiple pathways.

The autophagy-dependent pathway may be responsible for the regulation of microglial polarization. Autophagy is a self-eating cellular catabolic pathway that maintains cellular homeostasis by degrading long-lived proteins, damaged organelles, and misfolded proteins after hypoxia [77,78]. Western blotting was used to analyze the expression of autophagy-related proteins in the brains of MCAO rats (Fig. 7J and S10A-S10D). Lipo@GB-DHA can promote the p-TAK1-dependent activation of p-AMPK, which is a regulator of metabolism and autophagy [79]. The results were consistent with that both DHA and GB can upregulate the expression of p-AMPK in cells and tissues as reported [80,81]. Moreover, treatment with Lipo@GB-DHA noticeably promoted the expression of ATG5, an autophagy rate-related protein. Besides, the level of LC3II/I in the Lipo@GB-DHA group was higher than that in the MCAO and Sham groups, indicating an increase in autophagosomes. So, in this part, autophagy was most effectively activated by Lipo@GB-DHA, benefit for CI/RI.

These results suggested that the targeted delivery of Lipo@GB-DHA to the ischemic brain can alleviate

inflammation, maintain brain microenvironment homeostasis and angiogenesis.

3.9. *Safety evaluation of Lipo@GB-DHA*

Finally, the biosafety of Lipo@GB-DHA was evaluated in MCAO rats. After multiple administration of 5 mg/kg GB, all MCAO rats were found to be healthy. Moreover, changes in the major organs were examined by H&E staining, the results indicated that there were almost no distinguishable injuries in tissues (Fig. S11A). In addition, after the administration of Lipo@GB-DHA, the serum creatinine (CREA) and urea nitrogen (UREA) levels in the serum were similar to those in the Sham group, which were much lower than those in the MCAO group, indicating that Lipo@GB-DHA was safe (Fig. S11B-S11C). In summary, these results demonstrated the biocompatibility of Lipo@GB-DHA constructed in this study, both *in vitro* and *in vivo*.

4. Conclusion

In this study, a GB-DHA complex strategy was used to reverse the poor solubility and stability of GB in liposomes. And, finally constructed nanoliposomes (Lipo@GB-DHA) with stability, multi-functional and available for industrialization were engineered for the targeted treatment of CI/RI (Scheme.1). Here, GB-DHA-loaded liposomes with passive targeting ability can more accumulate in ischemic region than free solution. Furtherly, the intravenous injection of Lipo@GB-DHA was found to significantly decrease the infarct volume and notably ameliorate neurological impairment in MCAO rats both at 2 and 6 h post-reperfusion, which means a lot for delayed intervention of CI/RI in clinical.

Studies on mechanisms proved that Lipo@GB-DHA could play an important role in ROS scavenging, so as to decoy neuron apoptosis and down-regulate the secretion of pro-inflammatory cytokines after hypoxia-reoxygenation process. Besides, Lipo@GB-DHA seems to do some helps to neurovascular units remodeling by polarizing microglia from M1 to “tissue-repairing” M2 phenotype to stimulate angiogenesis, activating autophagy to maintain homeostasis. Therefore, compared to the injection currently available on the market, Lipo@GB-DHA could provide a new option for regulating multiple events during stroke. However, challenges still exist in its clinical transformation, including still low intracerebral distribution and safety considerations. So, in the future, further research will be needed.

Conflicts of interest

The authors report no conflicts of interest. The authors are responsible for the content and writing of this paper.

Acknowledgements

We thank the staff members of Integrated Laser Microscopy System at the National Facility for Protein Science in Shanghai (NFPS) for providing technical support and assistance in data collection and analysis. We thank the all members in Guo Wei’s Lab for the use of anoxic incubator. This research was funded by the National Natural Science Foundation of China (No.81773911, 81690263 and 81573616), the Development Project of Shanghai Peak Disciplines-Integrated Medicine (No.20180101).

Supplementary materials

Supplementary material associated with this article can be found, in the online version, at doi:10.1016/j.ajps.2023.100783.

References

[1] The top 10 causes of death. Available from: https://www.who.int/news-room/fact-sheets/detail/the-top-10-causes-of-death.
[2] Shi K, Tian DC, Li ZG, Ducruet AF, Lawton MT, Shi FD. Global brain inflammation in stroke. Lancet Neurol 2019;18(11):1058–66.
[3] Mizuma A, You JS, Yenari MA. Targeting reperfusion injury in the age of mechanical thrombectomy. Stroke 2018;49(7):1796–802.
[4] Green AR, Hainsworth AH, Jackson DM. GABA potentiation: a logical pharmacological approach for the treatment of acute ischaemic stroke. Neuropharmacology 2000;39(9):1483–94.
[5] Dabrowska S, Andrzejewska A, Lukomska B, Janowski M. Neuroinflammation as a target for treatment of stroke using mesenchymal stem cells and extracellular vesicles. J Neuroinflammation 2019;16(1):178.
[6] Li M, Li J, Chen J, Liu Y, Cheng X, Yang F, et al. Platelet membrane biomimetic magnetic nanocarriers for targeted delivery and in situ generation of nitric oxide in early ischemic stroke. ACS Nano 2020;14(2):2024–35.
[7] Rajeev V, Fann DY, Dinh QN, Kim HA, De Silva T M, Lai MKP, et al. Pathophysiology of blood brain barrier dysfunction during chronic cerebral hypoperfusion in vascular cognitive impairment. Theranostics 2022;12(4):1639–58.
[8] Feng Z, Sun Q, Chen W, Bai Y, Hu D, Xie X. The neuroprotective mechanisms of ginkgolides and bilobalide in cerebral ischemic injury: a literature review. Mol Med 2019;25(1):57.
[9] Zhou JM, Gu SS, Mei WH, Zhou J, Wang ZZ, Xiao W. Ginkgolides and bilobalide protect BV2 microglia cells against OGD/reoxygenation injury by inhibiting TLR2/4 signaling pathways. Cell Stress Chaperon 2016;21(6):1037–53.
[10] Li S, Zhang X, Fang Q, Zhou J, Zhang M, Wang H, et al. Ginkgo biloba extract improved cognitive and neurological functions of acute ischaemic stroke: a randomised controlled trial. Stroke Vasc Neurol 2017;2(4):189–97.
[11] Li C, Liu K, Liu S, Aerqin Q, Wu X. Role of ginkgolides in the inflammatory immune response of neurological diseases: a review of current literatures. Front Syst Neurosci 2020;14:45.
[12] Wei H, Sun T, Tian Y, Wang K. Ginkgolide B modulates BDNF expression in acute ischemic stroke. J Korean Neurosurg Soc 2017;60(4):391–6.
[13] Zheng PD, Mungur R, Zhou HJ, Hassan M, Jiang SN, Zheng JS. Ginkgolide B promotes the proliferation and differentiation of neural stem cells following cerebral ischemia/reperfusion injury, both *in vivo* and *in vitro*. Neural Regen Res 2018;13(7):1204–11.
[14] Xiang Y, Yang N, Guo Z, Zhou L, Guo JJ, Hu M. Cost-effectiveness analysis of ginkgolide injection in the

treatment of ischemic stroke based on a randomized clinical trial. J Altern Complement Med 2021;27(4):331–41.
[15] Fang W, Deng Y, Li Y, Shang E, Fang F, Lv P, et al. Blood brain barrier permeability and therapeutic time window of Ginkgolide B in ischemia-reperfusion injury. Eur J Pharm Sci 2010;39(1-3):8–14.
[16] Allen TM, Cullis PR. Liposomal drug delivery systems: from concept to clinical applications. Adv Drug Deliv Rev 2013;65(1):36–48.
[17] Al-Ahmady ZS, Jasim D, Ahmad SS, Wong R, Haley M, Coutts G, et al. Selective liposomal transport through blood brain barrier disruption in ischemic stroke reveals two distinct therapeutic opportunities. ACS Nano 2019;13(11):12470–86.
[18] Terstappen GC, Meyer AH, Bell RD, Zhang W. Strategies for delivering therapeutics across the blood-brain barrier. Nat Rev Drug Discov 2021;20(5):362–83.
[19] Knowland D, Arac A, Sekiguchi KJ, Hsu M, Lutz S E, Perrino J, et al. Stepwise recruitment of transcellular and paracellular pathways underlies blood-brain barrier breakdown in stroke. Neuron 2014;82(3):603–17.
[20] Jablonsky M, Haz A, Burcova Z, Kreps F, Jablonsky J. Pharmacokinetic properties of biomass-extracted substances isolated by green solvents. BioResources 2019;14(3):6294–303.
[21] Thid D, Benkoski JJ, Svedhem S, Kasemo B, Gold J. DHA-induced changes of supported lipid membrane morphology. Langmuir 2007;23(11):5878–81.
[22] Shi L, Wang Y, Wang Q, Jiang Z, Ren L, Yan Y, et al. Transforming a toxic drug into an efficacious nanomedicine using a lipoprodrug strategy for the treatment of patient-derived melanoma xenografts. J Control Release 2020;324:289–302.
[23] Bu J, Dou Y, Tian X, Wang Z, Chen G. The role of omega-3 polyunsaturated fatty acids in stroke. Oxid Med Cell Longev 2016;2016:6906712.
[24] Yang YC, Lii CK, Wei YL, Li CC, Lu CY, Liu KL, et al. Docosahexaenoic acid inhibition of inflammation is partially via cross-talk between Nrf2/heme oxygenase 1 and IKK/NF-κB pathways. J Nutr Biochem 2013;24(1):204–12.
[25] Cai W, Liu S, Hu M, Sun X, Qiu W, Zheng S, et al. Post-stroke DHA treatment protects against acute ischemic brain injury by skewing macrophage polarity toward the M2 Phenotype. Transl Stroke Res 2018;9(6):669–80.
[26] Valentine RC, Valentine DL. Omega-3 fatty acids in cellular membranes: a unified concept. Prog Lipid Res 2004;43(5):383–402.
[27] Li G, Li Y, Xiao B, Cui D, Lin Y, Zeng J, et al. Antioxidant activity of docosahexaenoic acid (DHA) and its regulatory roles in mitochondria. J Agric Food Chem 2021;69(5):1647–55.
[28] Luo C, Sun J, Sun B, Liu D, Miao L, Goodwin T J, et al. Facile fabrication of tumor redox-sensitive nanoassemblies of small-molecule oleate prodrug as potent chemotherapeutic nanomedicine. Small 2016;12(46):6353–62.
[29] Hu L, Chen Z, Xie Y, Jiang Y, Zhen H. Alkyl and alkoxycarbonyl derivatives of ginkgolide B: synthesis and biological evaluation of PAF inhibitory activity. Bioorg Med Chem 2000;8(6):1515–21.
[30] Zhang LL, Zhu YF, Wei XB, et al. Nanoplateletsomes restrain metastatic tumor formation through decoy and active targeting in a preclinical mouse model. Acta Pharmaceutica Sinica B 2022;12(8):3427–47.
[31] Zhang H. Thin-film hydration followed by extrusion method for liposome preparation. Methods Mol Biol 2017;1522:17–22.
[32] Nagashima K, Zheng J, Parmiter D, Patri AK. Biological tissue and cell culture specimen preparation for TEM nanoparticle characterization. Methods Mol Biol 2011;697:83–91.
[33] Grabielle-Madelmont C, Lesieur S, Ollivon M. Characterization of loaded liposomes by size exclusion chromatography. J Biochem Biophys Methods 2003;56(1-3):189–217.
[34] Wang S, Gan Y, Kan H, Mao X, Wang Y. Exploitation of HPLC analytical method for simultaneous determination of six principal unsaturated fatty acids in oviductus ranae based on quantitative analysis of multi-components by single-marker (QAMS). Molecules 2021;26(2):479.
[35] Nguyen TL, Nguyen TH, Nguyen DH. Development and *in vitro* evaluation of liposomes using soy lecithin to encapsulate paclitaxel. Int J Biomater 2017;2017:8234712.
[36] Lu Y, Li C, Chen Q, Liu P, Guo Q, Zhang Y, et al. Microthrombus-targeting micelles for neurovascular remodeling and enhanced microcirculatory perfusion in acute ischemic stroke. Adv Mater 2019;31(21):e1808361.
[37] Zeng F, Wu Y, Li X, Ge X, Guo Q, Lou X, et al. Custom-made ceria nanoparticles show a neuroprotective effect by modulating phenotypic polarization of the microglia. Angew Chem Int Ed Engl 2018;57(20):5808–12.
[38] Eruslanov E, Kusmartsev S. Identification of ROS using oxidized DCFDA and flow-cytometry. Methods Mol Biol 2010;594:57–72.
[39] Lian H, Roy E, Zheng H. Protocol for primary microglial culture preparation. Bio Protoc 2016;6(21):e1989.
[40] Tamashiro TT, Dalgard CL, Byrnes KR. Primary microglia isolation from mixed glial cell cultures of neonatal rat brain tissue. J Vis Exp 2012(66):e3814.
[41] Yan H, MiX Midgley AC, Du X, Huang Z, Wei T, et al. Targeted repair of vascular injury by adipose-derived stem cells modified with P-selectin binding peptide. Adv Sci (Weinh) 2020;7(11):1903516.
[42] Lässer C, Eldh M, Lötvall J. Isolation and characterization of RNA-containing exosomes. J Vis Exp 2012(59):e3037.
[43] Wu HH, Jiang XC, Li YS, Zhou Y, Zhang TY, Zhi P, et al. Engineering stem cell derived biomimetic vesicles for versatility and effective targeted delivery. Adv Funct Mater 2020;30(49):2006169.
[44] Wang H, Xu X, Guan X, Shen S, Huang X, Kai G, et al. Liposomal 9-aminoacridine for treatment of ischemic stroke: from drug discovery to drug delivery. Nano Lett 2020;20(3):1542–51.
[45] Qu G, Wang X, Liu Q, Liu R, Yin N, Ma J, et al. The ex vivo and *in vivo* biological performances of graphene oxide and the impact of surfactant on graphene oxide's biocompatibility. J Environ Sci (China) 2013;25(5):873–81.
[46] He W, Mei Q, Li J, Zhai Y, Chen Y, Wang R, et al. Preferential targeting cerebral ischemic lesions with cancer cell-inspired nanovehicle for ischemic stroke treatment. Nano Lett 2021;21(7):3033–43.
[47] Benedek A, Móricz K, Jurányi Z, Gigler G, Lévay G, Hársing LG Jr, et al. Use of TTC staining for the evaluation of tissue injury in the early phases of reperfusion after focal cerebral ischemia in rats. Brain Res 2006;1116(1):159–65.
[48] Frank D, Gruenbaum BF, Grinshpun J, Melamed I, Severynovska O, Kuts R, et al. Measuring post-stroke cerebral edema, infarct zone and blood-brain barrier breakdown in a single set of rodent brain samples. J Vis Exp 2020;164.
[49] Chen SH, Qiu QQ, Wang DD, She DJ, Chai ML, He HN, et al. Long acting carmustine loaded natural extracellular matrix hydrogel for inhibition of glioblastoma recurrence after tumor resection. Front Chem Sci Eng 2022;16:536–45.
[50] Martin E, El-Behi M, Fontaine B, Delarasse C. Analysis of microglia and monocyte-derived macrophages from the central nervous system by flow cytometry. J Vis Exp 2017(124):e55781.
[51] Campanella M, Sciorati C, Tarozzo G, Beltramo M. Flow cytometric analysis of inflammatory cells in ischemic rat brain. Stroke 2002;33(2):586–92.
[52] Xia Y, Hu G, Chen Y, Yuan J, Zhang J, Wang S, et al. Embryonic stem cell derived small extracellular vesicles modulate regulatory T cells to protect against ischemic stroke. ACS Nano 2021;15(4):7370–85.

[53] Mitsios N, Gaffney J, Krupinski J, Mathias R, Wang Q, Hayward S, et al. Expression of signaling molecules associated with apoptosis in human ischemic stroke tissue. Cell Biochem Biophys 2007;47(1):73–86.
[54] Liu M, Boussetta T, Makni-Maalej K, Fay M, Driss F, El-Benna J, et al. Protectin DX, a double lipoxygenase product of DHA, inhibits both ROS production in human neutrophils and cyclooxygenase activities. Lipids 2014;49(1):49–57.
[55] Briuglia ML, Rotella C, McFarlane A, Lamprou DA. Influence of cholesterol on liposome stability and on *in vitro* drug release. Drug Deliv Transl Res 2015;5(3):231–42.
[56] Varbo A, Nordestgaard BG, Tybjaerg-Hansen A, Schnohr P, Jensen GB, Benn M. Nonfasting triglycerides, cholesterol, and ischemic stroke in the general population. Ann Neurol 2011;69(4):628–34.
[57] Dittgen M, Herbst B. Zeta potential–fundamentals, measurement methods and application to pharmacy. Pharmazie 1987;42(10):641–56.
[58] Derksen J, Meekes H. Selective staining of nucleic acid containing structures by uranyl acetate-lead citrate. Micron and Microscopica Acta 1984;15:55–8.
[59] Granger DN, Kvietys PR. Reperfusion injury and reactive oxygen species: the evolution of a concept. Redox Biol 2015;6:524–51.
[60] Jeong SY, Seol DW. The role of mitochondria in apoptosis. BMB Rep 2008;41(1):11–22.
[61] Simon HU, Haj-Yehia A, Levi-Schaffer F. Role of reactive oxygen species (ROS) in apoptosis induction. Apoptosis 2000;5(5):415–18.
[62] Hu X, Li P, Guo Y, Wang H, Leak RK, Chen S, et al. Microglia/macrophage polarization dynamics reveal novel mechanism of injury expansion after focal cerebral ischemia. Stroke 2012;43(11):3063–70.
[63] Zhang Y, Zhao Y, Zhang J, Gao Y, Li S, Chang C, et al. Ginkgolide B inhibits NLRP3 inflammasome activation and promotes microglial M2 polarization in Aβ (1-42)-induced microglia cells. Neurosci Lett 2021;764:136206.
[64] Kawano A, Ariyoshi W, Yoshioka Y, Hikiji H, Nishihara T, Okinaga T. Docosahexaenoic acid enhances M2 macrophage polarization via the p38 signaling pathway and autophagy. J Cell Biochem 2019;120(8):12604–17.
[65] Lu H, Li S, Dai D, Zhang Q, Min Z, Yang C, et al. Enhanced treatment of cerebral ischemia-Reperfusion injury by intelligent nanocarriers through the regulation of neurovascular units. Acta Biomater 2022;147:314–26.
[66] Singh RD, Puri V, Valiyaveettil JT, Marks DL, Bittman R, Pagano RE. Selective caveolin-1-dependent endocytosis of glycosphingolipids. Mol Biol Cell 2003;14(8):3254–65.
[67] Mullen A, Loscher CE, Roche HM. Anti-inflammatory effects of EPA and DHA are dependent upon time and dose-response elements associated with LPS stimulation in THP-1-derived macrophage. J Nutr Biochem 2010;21(5):444–50.
[68] Sydserff SG, Borelli AR, Green AR, Cross AJ. Effect of NXY-059 on infarct volume after transient or permanent middle cerebral artery occlusion in the rat; studies on dose, plasma concentration and therapeutic time window. Br J Pharmacol 2002;135(1):103–12.
[69] Yu WB, Cao L, Zhao YY, Xiao W, Xiao BG. Comparing the role of Ginkgolide B and Ginkgolide K on cultured astrocytes exposed to oxygenglucose deprivation. Mol Med Rep 2018;18(5):4417–27.
[70] Jin R, Yang G, Li G. Inflammatory mechanisms in ischemic stroke: role of inflammatory cells. J Leukoc Biol 2010;87(5):779–89.
[71] Planas AM. Role of immune cells migrating to the ischemic brain. Stroke 2018;49(9):2261–7.
[72] Short WD, Steen E, Kaul A, Wang X, Olutoye OO 2nd, Vangapandu HV, et al. Il-10 promotes endothelial progenitor cell infiltration and wound healing via stat3. Faseb J 2022;36(7):e22298.
[73] Nakamura R, Sene A, Santeford A, Gdoura A, Kubota S, Zapata N, et al. IL10-driven STAT3 signalling in senescent macrophages promotes pathological eye angiogenesis. Nat Commun 2015;6:7847.
[74] Dace DS, Khan A A, Kelly J, Apte RS. Interleukin-10 promotes pathological angiogenesis by regulating macrophage response to hypoxia during development. PLoS One 2008;3(10):e3381.
[75] Zhang XJ, Liu X, Hu M, Zhao GJ, Sun D, Cheng X, et al. Pharmacological inhibition of arachidonate 12-lipoxygenase ameliorates myocardial ischemia-reperfusion injury in multiple species. Cell Metab 2021;33(10):2059–75.
[76] Zheng Z, Li Y, Jin G, Huang T, Zou M, Duan S. The biological role of arachidonic acid 12-lipoxygenase (ALOX12) in various human diseases. Biomed Pharmacother 2020;129:110354.
[77] Zhuang X, Yu Y, Jiang Y, Zhao S, Wang Y, Su L, et al. Molecular hydrogen attenuates sepsis-induced neuroinflammation through regulation of microglia polarization through an mTOR-autophagy-dependent pathway. Int Immunopharmacol 2020;81:106287.
[78] Wang P, Shao BZ, Deng Z, Chen S, Yue Z, Miao CY. Autophagy in ischemic stroke. Prog Neurobiol 2018;163-164:98–117.
[79] Jia J, Bissa B, Brecht L, Allers L, Choi SW, Gu Y, et al. AMPK, a regulator of metabolism and autophagy, is activated by lysosomal damage via a novel galectin-directed ubiquitin signal transduction system. Mol Cell 2020;77(5):951–69 e9.
[80] Yu WB, Cao L, Zhao YY, Xiao W, Xiao BG. Comparing the role of Ginkgolide B and Ginkgolide K on cultured astrocytes exposed to oxygenglucose deprivation. Mol Med Rep 2018;18(5):4417–27.
[81] Jing K, Song KS, Shin S, Kim N, Jeong S, Oh HR, et al. Docosahexaenoic acid induces autophagy through p53/AMPK/mTOR signaling and promotes apoptosis in human cancer cells harboring wild-type p53. Autophagy 2011;7(11):1348–58.